**Czech Technical University in Prague**
**Faculty of Nuclear Sciences and Physical Engineering**
**Department of Physics**
**Study branch: Physics and Technology of Nuclear Fusion**

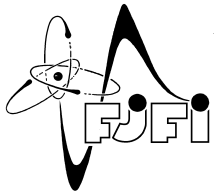


# Measurement of edge plasma density by energetic beam of Li atoms on the COMPASS tokamak

DIPLOMA THESES

Author: Bc. Jaroslav Krbec
Supervisor: RNDr. Jan Stöckel, CSc.
Consultant: Dr. Miklós Berta
Year: 2013

zadání podepsané děkanem

zadní strana zadání podepsané děkanem

**Prohlášení**

Prohlašuji, že jsem svou diplomovou práci vypracoval samostatně a použil jsem pouze podklady (literaturu, projekty, SW atd.) uvedené v přiloženém seznamu.

Nemám závažný důvod proti užití tohoto školního díla ve smyslu § 60 Zákona č.121/2000 Sb., o právu autorském, o právech souvisejících s právem autorským a o změně některých zákonů (autorský zákon).

V Praze dne .....

.....
Bc. Jaroslav Krbec

*Název práce:*

**Měření hustoty okrajového plazmatu pomocí energetického svazku Li atomů na tokamaku COMPASS**

*Autor:* Bc. Jaroslav Krbec

*Obor:* Fyzikální inženýrství
*Druh práce:* Diplomová práce

*Vedoucí práce:* RNDr. Jan Stöckel, CSc.
Ústav fyziky plazmatu, AV ČR, v.v.i.
*Konzultant:* Dr. Miklós Berta
Széchenyi István University, Győr, Maďarsko

*Abstrakt:*
Tato práce se zabývá rekonstrukcí hustoty okrajového plazmatu ze záření produkovaného interakcí energetického svazku Li atomů s plazmatem. K měření byla použita CCD kamera s optickým filtrem (670,8 nm) a časovým rozlišením 20 ms.
V rámci teoretické části jsou shrnuty základní informace o experimentálním uspořádání a diagnostice BES a je popsán rekonstrukční program implementovaný v prostředí MATLAB. V experimentální části je popsáno testování svazku a jsou ukázány výsledky rekonstrukcí pro data naměřená na COMPASSu a TEXTORu.

*Klíčová slova:* lithový svazek, rekonstrukce hustoty plazmatu, BES, COMPASS

*Title:*

**Measurement of edge plasma density by energetic beam of Li atoms on the COMPASS tokamak**

*Author:* Bc. Jaroslav Krbec

*Abstract:*
This work deals with reconstruction of edge plasma density from radiation of energetic Li atoms caused by its interaction with plasma. The measurement was realized by CCD camera equipped with optic filter (670,8 nm) with time resolution 20ms.
In theoretical part of this theses, the information about experimental setup and BES diagnostic was summarized and the reconstruction algorithm implemented in MATLAB enviroment was described. In the experimental part of this theses, the beam testing results and reconstructed plasma profiles from COMPASS and TEXTOR tokamak were shown.

*Key words:* Li-beam, BES, plasma density reconstruction, COMPASS

# Acknowledgements

My thanks for their helpful suggestions go to Miklós Berta, Jan Stöckel and Attila Bencze. I also thank Dániel Réfy for TEXTOR data, not least all those who have developed and tested Li-beam device.

# Contents

# List of Figures

# List of Tables

# Glossary

**ABP** Atomic Beam Probe; a new approach for measurement of the current in the edge plasma, system uses neutral lithium diagnostic beam injected into the plasma

**APD** Avalanche Photodiode; a semiconductor photodetector, high reverse bias voltage provides current gain (100 - 1000) due to impact ionization (avalanche effect)

**BES** Beam Emission Spectroscopy; a diagnostic method observes the spatial and temporal variation of the lithium radiation from the beam for purposes of measuring density perturbations

**CXRS** Charge Exchange Recombination Spectroscopy; a diagnostic method detecting light emitted by the ions in plasma which captured electron form the neutral atom injected to the tokamak chamber (typically by NBI)

**EBW** Electron Bernstein Wave;

**ECE** Electron Cyclotron Emission; a radiation emitted by electrons as a result of their cyclotron motion around magnetic field lines, used to measure electron temperature

**ELM** Edge Localised Modes; an instability which occurs in short periodic bursts during the H-mode in divertor tokamaks

**HFS** High Field Side; a side of the plasma column with higher toroidal field

**HIBP** Heavy Ion Beam Probe; a diagnostic for measurement of electron density, poloidal magnetic field and electric potencial using heavy ions (typically Cesium)

**ICRH** Ion Cyclotron Resonance Heating; a system for heating ions using absorption of an electromagnetic radiation at frequency of ion circular movement in magnetic field

**IPP** Institute of Plasma Physics AS CR, v.v.i.

**ITER** International Thermonuclear Experimental Reactor; an international nuclear fusion research and engineering project, the world's largest and most advanced experimental tokamak nuclear fusion reactor under construction

**LCFS** Last Closed Flux Surface; a magnetic flux surface which doesn't intersect a tokamak chamber

**LHCD** Lower Hybrid Current Drive;

**LHW** Lower Hybrid Wave;

**MHD** Magnetohydrodynamics; a physical theory which describes the dynamics of electrically conducting fluids

**NBI** Neutral Beam Injection; a system for injection of hydrogen atoms and it's isotopes used for plasma heating and diagnostic

**PDF** Probability density function;

## GLOSSARY

**RMKI** Részecske- és Magfizikai Kutatóintézet; Research Institute for Particle and Nuclear Physics

**SOL** Scrape-off layer; a plasma region outside the last closed flux surface (LCFS)

**SXR** Soft X-Ray; an electromagnetic radiation with a wavelength in the range of 10 to 0.10 nanometers

**XR** X-Ray; an electromagnetic radiation with a wavelength in the range of 10 to 0.01 nanometers

**XUV** Extreme Ultraviolet; an electromagnetic radiation with a wavelength in the range of 100 to 10 nm

# 1

# Introduction

The aim of fusion research is to provide a source of heat, electricity and neutrons for the society in the future. At present an electric energy is mostly obtained from the shrinking supplies of raw materials and from nuclear power plants. The increase of electric energy consumption is expected due to growing population and increasing of standard of living in developing countries [31]. The scientists have learned how to control a fusion reaction by processes which take place in the stars. There are atomic nuclei join together under conditions of high density and temperature in the stars. The gravitational force was replaced by magnetic fields which confine plasma in laboratories and research centers. A device called tokamak is one of the devices which showed significant progress in achieving the desired parameters for thermonuclear fusion during the last few decades.

A tokamak (acronym of russian words: TOroidal'naya KAmera s MAgnitnymi Katushkami) was developed in the fifties of the 20th century by soviet physicists A. D. Sacharov, I. J. Tamm and L. A. Artsimovich. This device confines plasma in the torus chamber by the magnetic field. A tokamak 1.1 consists of a vacuum chamber in the shape of toroid representing a secondary winding of transformator and toroidal field coils which are wounded on the torus. A various support systems and diagnostic devices are essential parts of a tokamak. Additional heating of plasma is mainly realized by Ion Cyclotron Resonance Heating system, Electron Cyclotron Heating system and a Neutral Beam Injection system [35].

During the era of massive plasma heating to reach higher plasma temperature the scientist Fritz Wagner observed a radical growth of confinement time at tokamak ASDEX in 1982 [33]. This phenomenon has never been observed before. The regime advantages were higher confinement time and higher energy stored in the plasma that is why the regime was named H-mode. A new instability type called Edge Localized Mode was observed in H-mode plasma [38]. The bunch of plasma particles is thrown from the plasma to the chamber wall during ELM instability see figure 1.2. Particle losses associated with energy losses prevents achieving high plasma densities and the energetic particles hitting the chamber wall also reduce a chamber wall durability and also damage sensitive diagnostic systems. A creation of bunches is probably connected with plasma edge region. It is the reason why the edge plasma region measurement with high temporal resolution is necessary for understanding of the ELM generation mechanism.

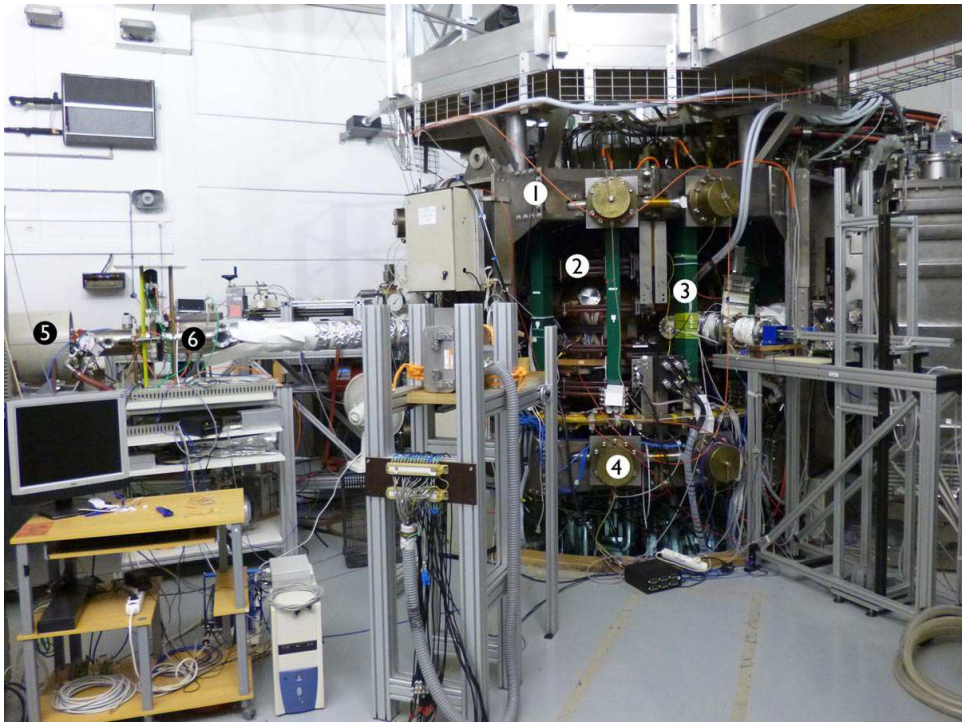


**Figure 1.1:** The COMPASS tokamak located in IPP.CR. Tokamak: 1. Main support struture, 2. Poloidal field coils, 3. Toroidal field coils, 4. Radial preload jacks. Lithium beam device: 5. Ion source and ion optics, 6. Neutralizator

A several diagnostic methods were created for plasma edge measurement: probe diagnostic, optical diagnostic with fast cameras, beam diagnostic and other. Thesis deals with diagnostic system which uses an injection of lithium atoms for measurement plasma parameters in the edge plasma region. At present the lithium beam device is installed on COMPASS tokamak.

Lithium beam can be used for two kinds of diagnostics:

- BES (Beam Emission Spectroscopy) [20] is used for electron density measurement in the plasma edge region. Injected lithium atoms are ionised and excited due to collisions with electrons and ions in plasma. Produced line radiation at wavelength 670.8 nm is detected by a CCD camera. An electron density profile can be reconstructed from the light intensity profile.

- ABP (Atomic Beam Probe) [4] is a new approach for electric current measurement in the plasma edge region. Ionized lithium atoms are trapped by magnetic field and detected by the ABP detector. The position of an ion at the detector is influenced by magnetic field integrated over the ion path. The average magnetic field could be calculated from the position of an ion at the detector grid of the ABP. A plasma density can be estimated from the number of captured ions.

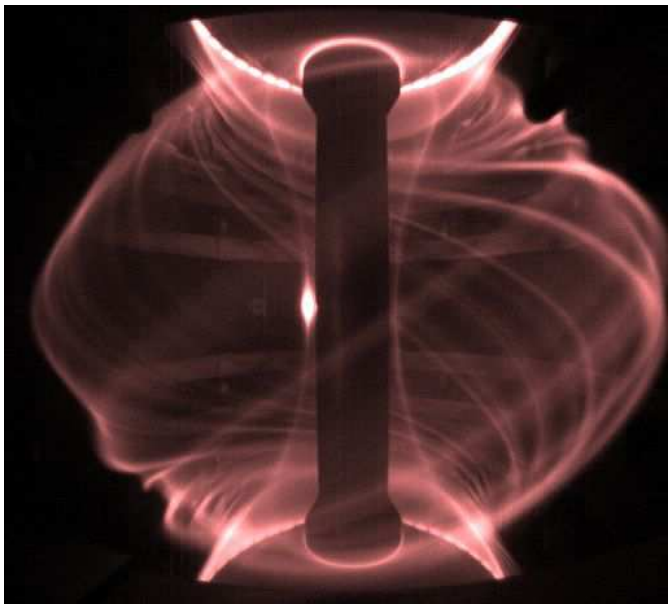

**Figure 1.2:** Filamentary structures observed during ELMs on the MAST tokamak [15].

The aim of the work is to summarize information about BES and lithium beam device and to show developed computer program for plasma density reconstruction and to compare reconstructed profiles with other diagnostics. The basic information about COMPASS tokamak and diagnostic systems installed on it are described at the beginning of the work. There is a description of the lithium beam device and Beam Emission Spectroscopy in second and third chapter respectively. The reconstruction method and results are shown at the end of the work.

# 2

# Tokamak COMPASS

## 2.1 History and parameters

The tokamak COMPASS (acronym for COMPact ASSembly) is a device developed in the 80's in Culham Science Center in England to study high-temperature plasma. The first plasma breakdown occurred in 1989 with circular cross section of the vacuum vessel [22]. The vacuum vessel was rebuilt to the D-shape cross section in 1992 and the tokamak was able to reach H-mode discharge [10] causing it to become one of the smallest tokamak with D-shape plasma which can operate in this regime. Due to its proportions (table 2.1) the COMPASS tokamak belongs among smaller tokamaks but the similar shape as ITER makes him a suitable device for studying ITER relevant behavior of plasma as shown in figure 2.1.

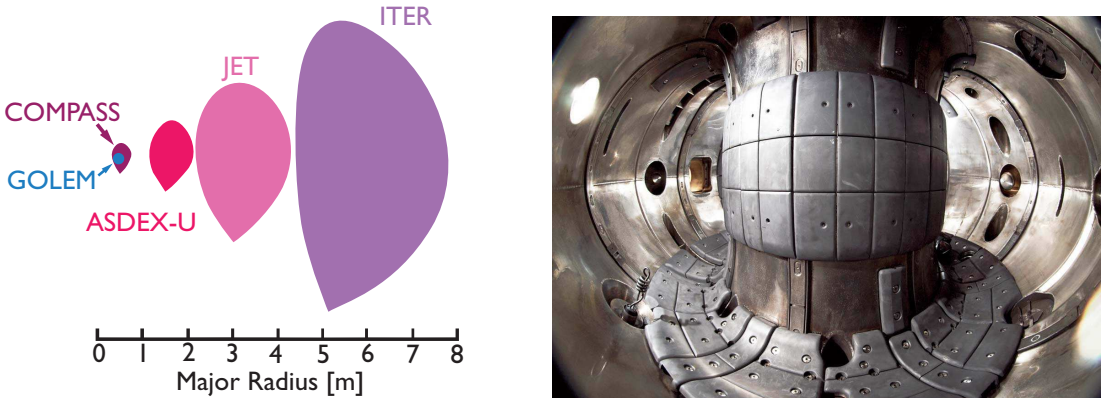


**Figure 2.1:** Left: A comparison of size and shape of the plasma cross section. Right: A picture of COMPASS chamber.

The tokamak was offered to Institute of Plasma Physics VV CR, v.v.i. in 2004 and it was decided to accept tokamak in 2005. The first plasma discharge in the tokamak took place in 2008 followed by installation of heating and diagnostics systems.

The tokamak is equipped by two NBI each with a power of 0.3 MW and by an antenna for Lower Hybrid Current Drive with power of 0.4 MW. Neutral Beam Injectors could be used in two configurations: (1) co-injection configuration and (2) balanced injection configuration which can produce non-rotating plasma which is very important because ITER plasma is expected to be non-rotating.

The basic parameters of tokamak are shown in table 2.1.

| Basic parameters of tokamak COMPASS [22] | |
|---|---|
| Major radius $R$ | 0,557 m |
| Minor radius, horizontal $a$ | 0,232 m |
| Minor radius, vertikal | 0,385 m |
| Aspect ration $R/a$ | 2,53 |
| Vessel material | Inconel 625 |
| Divertor material | Grafite |
| Maximal toroidal field on axis $B_T$ | 1,15 - 2,1 T |
| Maximal plasma current $I_p$ | 120 - 350 kA |
| Pulse duration | 300ms, max 1s |
| NBI $P_{NBI}$ 40 keV | 2x0,3 MW |
| Vacuum | $\sim 1{\cdot}10^{-8}$ Pa |

**Table 2.1:** Basic parameters of tokamak COMPASS.

## 2.2 Installed diagnostics

A following diagnostics will be used for plasma parameters measurement on COMPASS tokamak ([26], [34]):

- **Magnetic diagnostics:** A magnetic diagnostics belongs among basic diagnostics at every tokamak. A tokamak COMPASS is equipped with a 400 diagnostic coils for plasma current measurement, measurement of plasma shape, position and conductivity, MHD instabilities and plasma energy. A feedback control system uses plasma shape and position information to stabilize plasma and reach longer discharge. Magnetic surfaces reconstructed by EFIT code from magnetic coils signal are shown in figure 2.2.
- **Microwave diagnostics:** An electromagnetic radiation in microwave region is used to determinate properties of electrons in plasma. A tokamak is equipped with both active diagnostics (interferometer, reflectometer) and passive diagnostics (detection of microwave radiation from the plasma). There is a 2-mm interferometer used for line average electron density measurement and microwave reflectometer for electron density radial profile determination in plasma edge region. This density profile could be compared with reconstructed density profiles from lithium beam diagnostics. The radial profile of electron

temperature is obtained from ECE/EBW radiometer. The ECE/EBW diagnostics have to be absolutely calibrated e.g. by temperature measurement from Thomson scattering.

- **Spectroscopic diagnostics:** The spectroscopic diagnostics could be divided into two groups. Active diagnostics detect radiation which was produced by the interaction between plasma and particles (or radiation) which were delivered to the plasma by the experimentator. Passive diagnostics only detect the radiation and particles from plasma. The Thomson scattering [5] diagnostics belongs among the first group of diagnostics. It measures electron temperature and density. Following diagnostic devices belong to the second group:
  - fast camera [32] (32x1 px, sampling rate $\sim$ 140 kHz) observes the interaction between plasma and the chamber wall in visible spectrum
  - multichannel optical system used for plasma radiation measurement in the visible spectrum with the possibility to determine the time evolution of hydrogen and impurity radiation
  - bolometers (XUV) and SXR detector which serve for plasma radiation losses measurement
  - rotation of plasma is determined by the Doppler shift of carbon spectral line CIII i.e. $C^{2+}$ with wavelength 465 nm.
- **Beam & particle diagnostics:** The lithium beam diagnostics is used for two types of measurement in the plasma edge region: Beam Emission Spectroscopy detects line radiation which is emitted by injected lithium atoms. The BES could determine a radial profile of electron density and 2D electron density fluctuation profile in plasma edge region. The Atomic Beam Probe diagnostic detects deflection of lithium ions in the poloidal magnetic field using an ABP detector (rectangular grid of current detectors). This technique could determine a magnetic field perturbation and current profile in pedestal region. There is also used Neutral Particle Analyzer for analysis of the velocity distribution of neutral particles escaping from the plasma.
- **Probe diagnostics:** There will be several types of probes on the tokamak. A set of divertor Langmuir probes (39) is already working and measures electron density, electron temperature and floating potential in divertor region. This set of probes will be enhanced by 14 Langmuir probes on HFS. A two reciprocal probes (one with vertical and one with horizontal move) will measure the radial profile of electric plasma potential, electron density and temperature, particle flux from plasma to the chamber wall and ion temperature in the scrape-off layer. It is planned to insert a probe with diamond head even up to the pedestal region. The production and use of U-shape, sandwich and others probes are in progress.

The D-shape chamber in cooperation with a vertical field winding is able to form plasma to divertor configurations with both DND (double null D) and SND (single null) cross section.

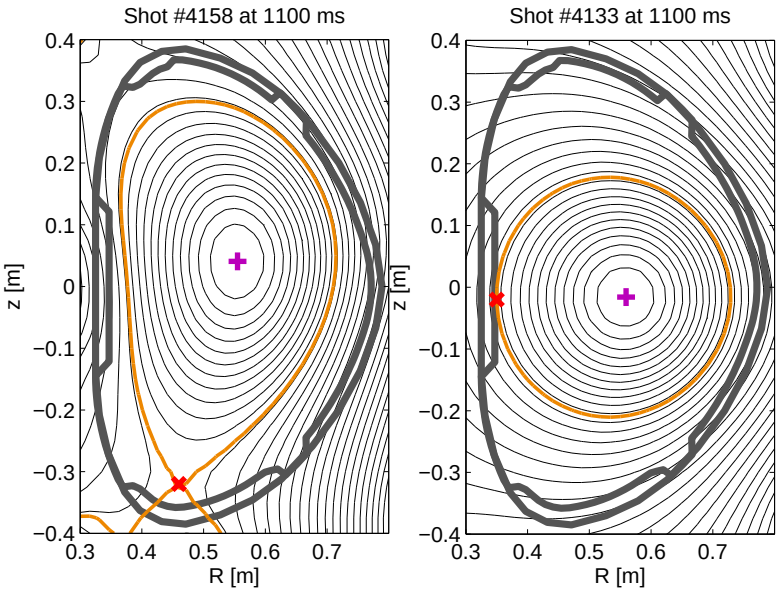


**Figure 2.2:** Reconstructed magnetic surfaces and LCFS (orange) from EFIT code [19]. Left picture: SNT configuration, Right picture: Circular plasma.

The most used profiles will be SND and SNT (higher triangularity) as shown in figure 2.2. It is possible to have both circular and D-shape cross section in limiter configurations.

L-H transition occurs in plasma with a SNT profile in which transport barrier is created and a region with high density gradient is produced in the edge plasma region which results in an increase of plasma density in the center.

The properties of L-H transition (i.e. threshold energy of L-H transition, hysteresis of L-H and H-L transition, width of pedestal) as well as edge region instabilities ELM and plasma turbulent behavior are the main research targets of tokamak COMPASS.

The other research subject is interaction between plasma and electromagnetic waves which consists of (1) study of interaction between Lower Hybrid Wave and plasma and phenomena close to LHW antenna, (2) use of Ion-cyclotron wave for plasma heating (ICRH) and (3) study of generation and detection of Electron-Bernstein waves. The research is also connected with advanced diagnostic methods such as:

1. Advanced electric probes for edge plasma parameters measurement (ion temperature, plasma potential and fluctuation).

2. New diagnostic methods for magnetic field measurement in tokamak/stelarator-like devices (Hall sensors).

3. Development of diagnostics for electron temperature and density measurement with high spatial resolution using Thomson scattering.

# 3

# Li-beam

There are some situations in which is very useful to use neutral beams consisting of atoms which are not typical for the fusion plasma. One advantage is that they can be relatively easily distinguished, usually spectroscopically, from the plasma species. The difficulty with many atoms, especially hydrogen, is that the transitions to and from their ground state are sufficiently energetic as to involve ultraviolet rather than visible radiation [14]. Because ultraviolet optic brings much more difficulties than the detection of visible light the lithium atoms are much more suitable. Most intensive lithium spectral line has length 670,8 nm. This gave a basics for lithium beam diagnostic. A lithium beam is a pure diagnostic device with power of approximately 100 W and atom energy $\sim$ 100keV which can be used for measurement of following plasma parameters:

1. Radial profile of electron density in the plasma edge region with spatial resolution of $\sim$ 1 cm and temporal resolution of $\sim$ 20 ms.
2. Two dimensional electron density fluctuation measurement in the plasma edge region which is closely connected with the study of anomalous particle transport and the study of particle poloidal flows and turbulent structures in the plasma edge region.
3. Measurement of magnetic field fluctuations and plasma current perturbation is a part of research on pedestal region behavior and ELM instability.
4. Measurement of magnetic field using the Zeeman effect on a lithium beam atoms and measurement of a field direction when the CW dye laser with rotating polarisation is used.

There will be usage of two diagnostic methods on tokamak COMPASS: (1) Beam Emission Spectroscopy and (2) Atomic Beam Probe diagnostics. The former is described in section 4 and the latter is briefly mentioned in section 3.4.

## 3.1 Principles

The lithium beam device consists of three main parts as shown in figure 3.1: (1) Ion source, (2) ion optics and (3) neutraliser.

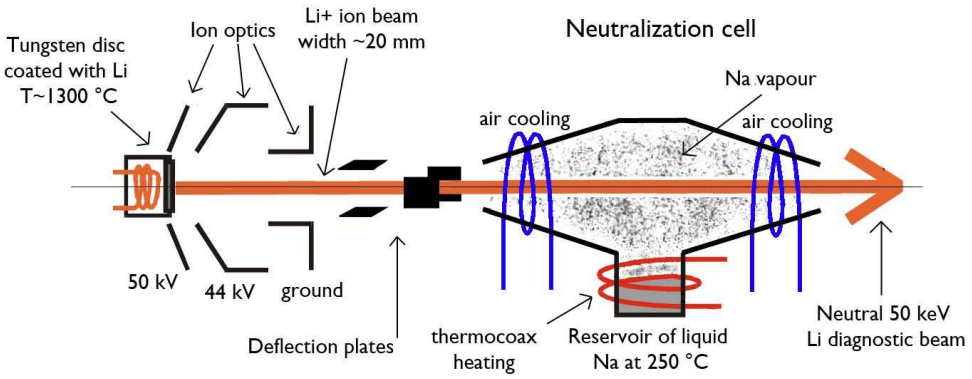


**Figure 3.1:** Schematic drawing of the lithium beam device. Figure taken from [7]

Lithium ions are emitted by heated anode (emitter). The emitter is composed of Li-$\beta$-eucryptite coated tungsten disc with a diameter of 19 mm which is inserted in molybdenum hollow. Maximal ion current is limited by two parameters: diffusivity and space charge. Diffusivity of material can be influenced by the temperature of the emitter. The emitter is heated by electric current up to a temperature of 1400 °C. A difference of voltage U1 and U2 represents an effective voltage applied to emitter which extracts lithium ions. A theoretical dependence of ion current on extracting voltage follows Child-Langmuir law

$$I = \frac{4\epsilon_0}{9}\sqrt{\frac{2e}{m}}\frac{U^{3/2}}{d^2}S \tag{3.1}$$

where $U$ is voltage between anode and cathode, $d$ is the distance between the anode and cathode, $e$ is the elementary charge, $m$ weight of Li-ion and $S$ surface of the anode as shown in figure 3.2. Current–voltage characteristic of emitter and Child-Langmuir law are shown in figure 3.2. There could be seen a saturation of emission current. This thermionic saturation current density depends on emitter temperature and is given by Richardson law:

$$j_{sat} = A_R T^2 \exp(\frac{-e\phi_R}{k_B T}) \tag{3.2}$$

where $A_R$ is the Richardson constant, $T$ is the temperature of the emitter, $e\phi$ is the work function, and $k_B$ is a Botlzmann constant.

A service of a beam highly depends on the operational lifetime of the emitter. This lifetime is influenced by emitting current. Extracted lithium ions are accelerated to the required energy and focused by ion optics. The ion optics consists of 4 electrically charged rings - emitter, extractor, puller and electron suppression ring and two pairs of deflecting plates. There are two voltages set in the accelerator. The main voltage between the puller and the emitter provides acceleration of the ion to the required energy and the voltage between emitter and extractor which represents an extraction voltage. The ratio of these voltages affects the focusation of the beam. There are two pairs of deflecting plates placed between accelerating and neutralizing

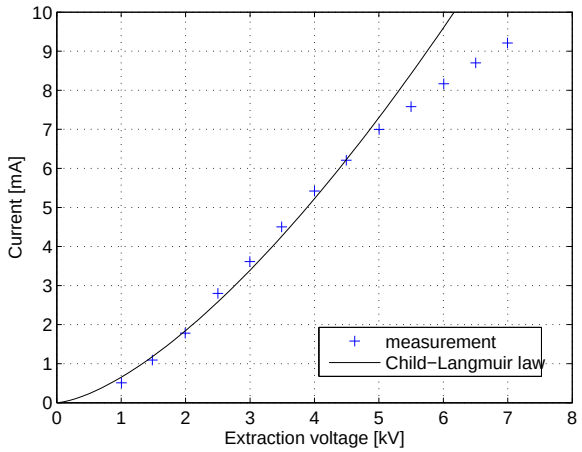


**Figure 3.2:** A total beam current according to extracting voltage. Figure taken from [2]

part. The first pair electrostatically deflects ions in vertical direction and is used for the beam sweeping in range of ±5cm in tokamak vessel to provide quasi 2D measurement and is also used for deflection to Faraday cup. The plasma background radiation is measured when the beam is deflected to Faraday cup. The sweeping frequency in the vertical direction can reach 400 kHz. The second pair of plates deflects ions in vertical direction. It serves for setting the optimal beam trajectory. The HV supply provides accelerating voltage up to 120 kV.

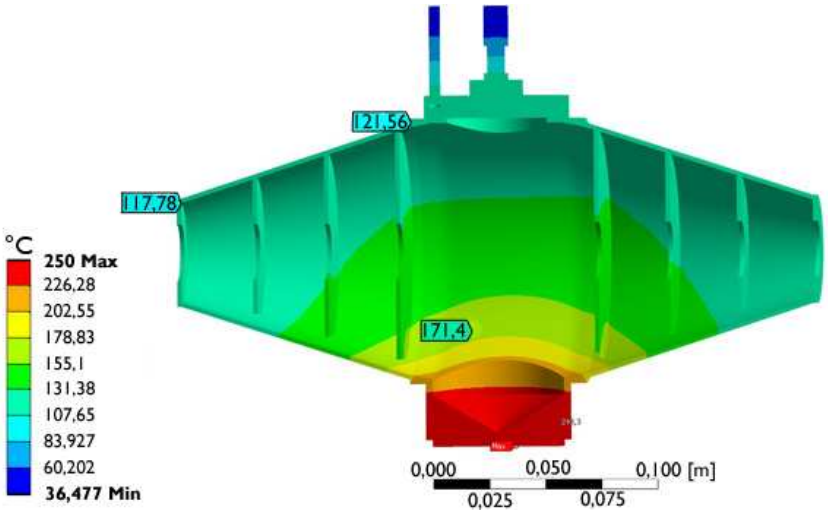


**Figure 3.3:** A temperature profile in neutralizer in steady state.

The lithium ions enter the neutralizer. The new concept of the neutralizer is used at tokamak COMPASS. The neutralizer consists of a reservoir of sodium and heater in its bottom part and

the tubes filled with cooling air wound on input and output part of neutralizer. Optimal heating (usually $\sim$ 250 °C) and cooling part setting causes evaporation of sodium in reservoir and its condensation in edge parts of neutralizer as shown in figure 3.3.

A liquid sodium flows back from the edge parts to the reservoir. The cooling parts minimize the leaks of sodium to other parts of Li-beam device and tokamak vessel. The lithium ion interacting in neutralizer with sodium gas gets an electron from neutral sodium atoms by charge exchange process. An ion undergoes a large amount of collisions in neutralizer because the interaction region is thick enough. This is the reason why the ratio of not-neutralized and neutralized ions is given by the ratio of reionization and charge exchange cross sections. Not-neutralized ions are deflected by magnetic field of tokamak and interact with flight tube wall. At the beginning there were few diaphragms in the flight tube in order to decrease the flow of sodium vapours to tokamak vessel but nowadays they are removed in order to prevent beam cropping. The accelerator, neutralizer with flight tube and tokamak are separated by valves and 3 turbomolecular pumps which provide a vacuum in this parts.

## 3.2 Experimental setup

Top and side view of the experimental setup at tokamak COMPASS is in figure 3.4 and 3.5. The CCD camera and ABP detector are installed on the top ports of the vacuum vessel. The avalanche photodiodes are installed on the bottom port.

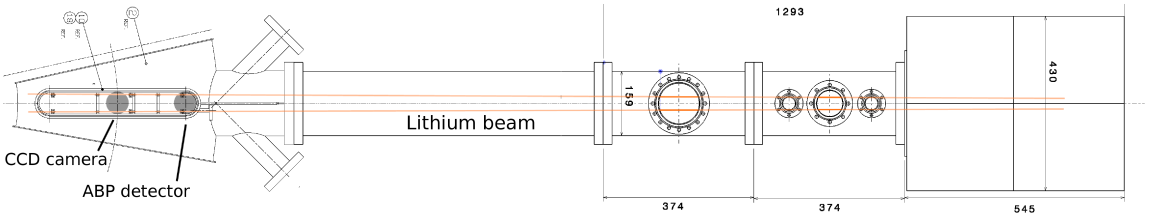


**Figure 3.4:** Experimental setup of lithium beam at tokamak COMPASS (top view).

## 3.3 BES diagnostics

### 3.3.1 CCD camera

The CCD camera is placed on the top port of the vacuum vessel. The CCD detector has resolution 640x480 px and temporal resolution 100 Hz. The temporal resolution could be higher at the expense of spatial resolution and amount of detected light. It is expected that 10 ms exposition time is going to be optimal. There are focusing optics and optical filter with center wavelength 670 nm with FWHM 10 nm. It is necessary to use a narrow filter because of small differences between observed lithium 2s-2p transition wavelength ($\lambda$ =670.8 nm) and $H_\alpha$ line (wavelength $\lambda$ =656.3 nm) and CII spectral line (wavelength $\lambda$ = 658 nm) which are the most intensive lines in the visible light spectrum at tokamak COMPASS.

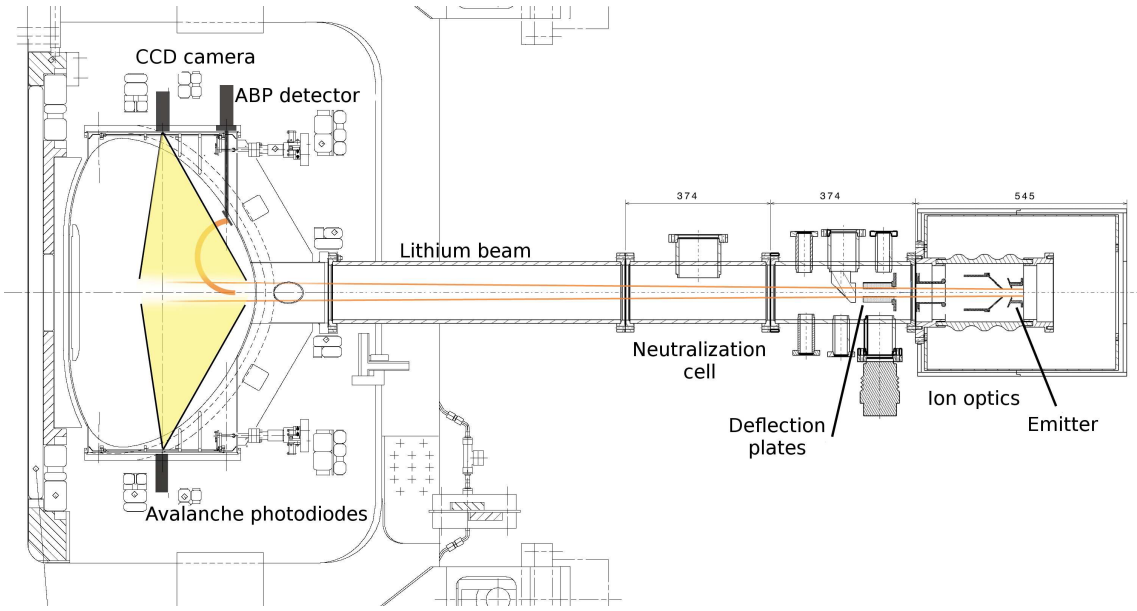


**Figure 3.5:** Experimental setup of lithium beam at tokamak COMPASS (side view).

### 3.3.2 APD detector

An array of avalanche photodiodes is installed on the bottom port of vacuum vessel in the same poloidal section as CCD camera and ABP detector. It is composed of 18 silicon detectors with effective surface of 25 $mm^2$ and temporal resolution of few $\mu$s. A quantum efficiency of the detector is $\sim 85\%$. The low-noise amplifier developed in RMKI is also part of the detector. The whole detector is placed in temperature-controlled housing.

## 3.4 ABP diagnostics

ABP is similar to the Heavy Ion Beam Probe (HIBP). The neutral lithium atoms are ionized during interaction with ions and electrons in plasma. The ion trajectory is curved due to the magnetic field and the ion impact on the ABP detector as shown in figure 3.6. The intensity of detected ions is proportional to the plasma density in the place of atom ionization and the shift of ions in toroidal direction is proportional to poloidal magnetic field integrated over the ion path.

### 3.4.1 ABP detector

The ABP detector is placed on the top port at the same poloidal section as a CCD camera. The head of ABP detector consists of twenty (4 x 5) copper plates which register all incident particles and of 4 Langmuir probes at the edge part of ABP head. The detector can be moved in the vertical direction for optimal position setting. The trial version of ABP detector is shown

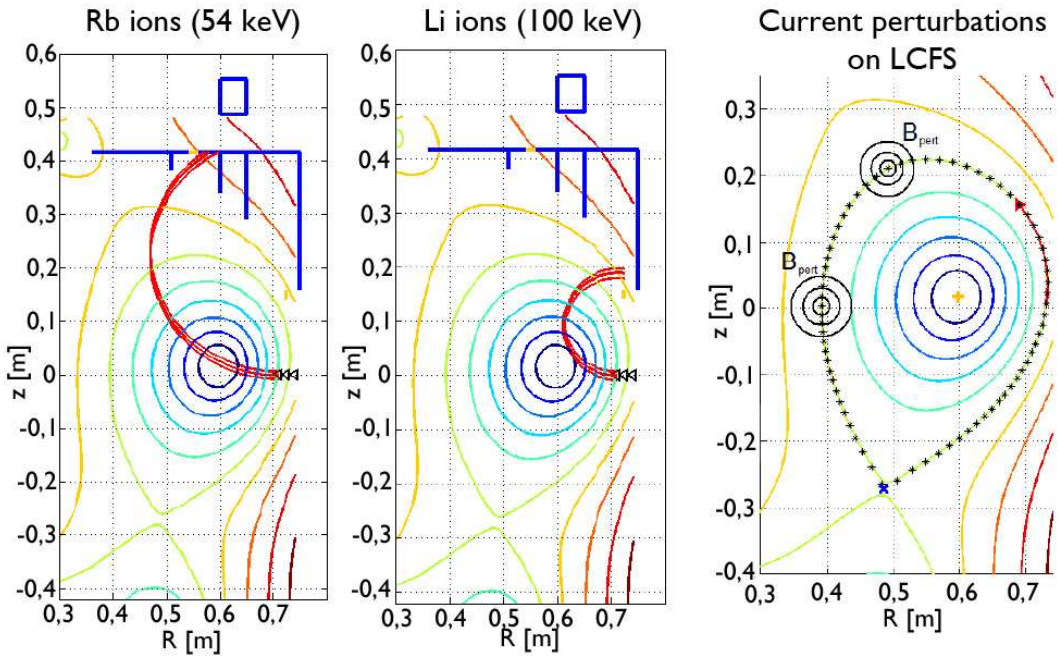


**Figure 3.6:** Simulation of $Rb^1+$ and $Li^1+$ trajectories. A figure taken from [4]

in figure 3.7. This detector is installed on tokamak and serves for noise intensity measurement. The original beam (with a diameter approximately 2 cm) will be cropped by diaphragm to the width of a few milimeters during ABP measurement. The planned head of ABP detector will have a copper segment 0.5 mm wide in the toroidal direction as shown in figure 3.7 and spatial resolution is expected to be approximately 0,1 mm. The spatial resolution corresponds to 10 kA plasma current which represents 5-10% of total plasma current at tokamak COMPASS.

## 3.5 Beam testing

It was decided to complete lithium beam device at the tokamak hall thus all the tests have to take place at the tokamak hall. There is a new type of neutralizer used in lithium beam device which has never been tested before and it can cause some unexpected issues. The goal of the lithium beam device is to transport enough lithium atoms to the tokamak chamber. The amount of lithium atoms transported into tokamak vessel depends on several parameters. The first one is the ion current $I_e$ obtained from the emitter. It is influenced by temperature of the emitter and extracting voltage (the difference between voltages $U_1$ and $U_2$ see picture 3.1). The second parameter is focusation of the beam. It is set by a ratio of voltages $U_1$ and $U_2$. The last parameter is neutralization efficiency which is influenced by a temperature of the sodium oven and a temperature of the neutralizer border area which is cooled by water. The resulting

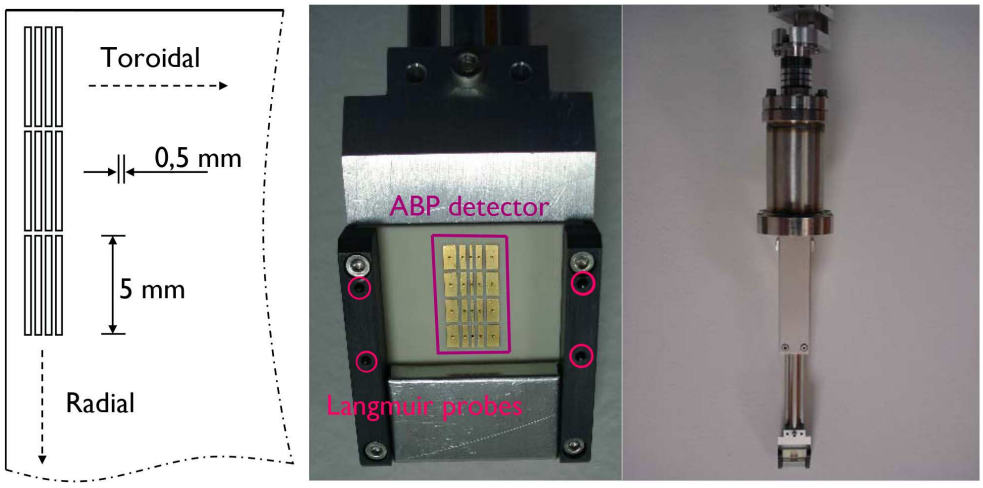


**Figure 3.7:** Left: Planned arrangement of probes on ABP detector. Middle and right: Trial version of ABP detector used at the tokamak. The figure taken from [13].

neutral lithium beam current $I_n$ which entrance tokamak vessel is given by

$$I_n = I_e(U_{ext}, T)\eta_f(U_1, U_2)\eta_n(T_{oven}, T_{edge}) \tag{3.3}$$

where $I_e$ is emitter current, $\eta_f(U_1, U_2)$ is focusing efficiency and $\eta_n(T_{oven}, T_{edge})$ is neutralization efficiency. A correct (optimal) voltages and temperatures for maximal lithium atom current must be found experimentally. There are next influences from a tokamak machine at the beam thus detailed testing for correct function of the beam is necessary.

### 3.5.1 Emitter and ion optic testing

The aim of measurement is to obtain maximal ion current at the end of flight tube. The ion current can be measured at the power source of accelerating voltage or by the Faraday cup (FC) at the end of flight tube. There are three parameters which influence the ion current: emitter temperature, extraction voltage $U_{ext} = U_1 - U_2$ and ratio of $U_1/U_2$ voltages. The ratio of voltages focuses a beam at the end of flight tube. The part of extracted ions is lost in device thus there is a difference between current measured at power source $U_1$ and Faraday cup as can be seen in table 3.1 and also the surface of FC.

The current was measured on FC with titanium plate and housing which can be charged by negative voltage to suppress electrons or by the positive voltage to pull up electrons. There can be also measured current on FC housing. The incidental ion can emit a few electrons from the Ti plate and these electrons can be measured on FC housing. The number of electrons produced by one ion ($e^-$ multiplication factor) can be calculated from the difference between FC Ti and FC housing current. The schematic drawing of FC is in figure 3.8.

Each emitter has a different volt-ampere characteristic. This characteristic has to follow Child-Langmuir law but for each emitter temperature exist a maximal extraction current limits.

| $U_1$ [kV] | $U_{ext}$ [kV] | $I_{ext}$ [mA] | $I_{FCTi}$ [mA] | $U_{FChousing}$ [V] | $I_{FChousing}$ [mA] | $\frac{I_{ext}}{I_{FCTi}}$ [mA] | $e^-$ multiplication factor |
|---|---|---|---|---|---|---|---|
| 10 | 1 | 0.083 | 0.067 | -500 | 0 | 0.81 | |
| | | | 0.34 | +500 | 0.26 | | 3.25 |
| 20 | 2 | 0.090 | 0.072 | -500 | 0 | 0.80 | |
| | | | 0.47 | +500 | 0.4 | | 5.75 |
| 30 | 3 | 0.100 | 0.075 | -500 | 0 | 0.75 | |
| | | | 0.55 | +500 | 0.47 | | 5.9 |
| 40 | 4 | 0.107 | 0.08 | -500 | 0 | 0.75 | |
| | | | 0.62 | +500 | 0.54 | | 6.8 |

**Table 3.1:** Measurement of faraday cup parameters (emitter heating current was 31 amps).

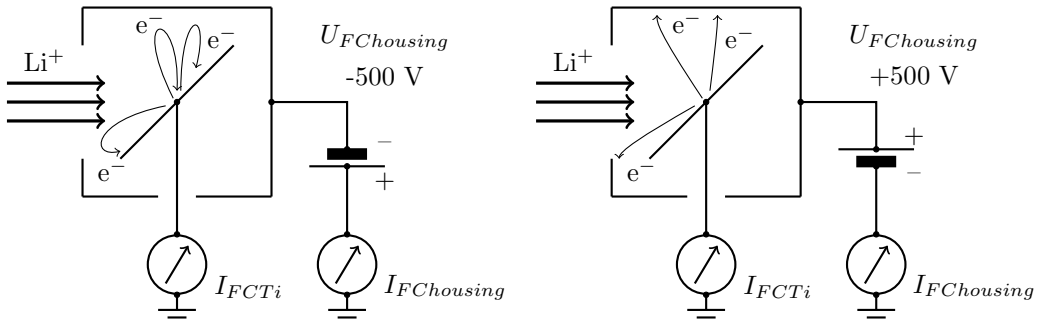


**Figure 3.8:** Schematic drawing of measurement with faraday cup, see table 3.1.

The current limit is clearly seen in figure 3.9. The emitter heating current is proportional to emitter temperature. The maximal current is 0.5 mA for heating current 46 amps and 1.8 mA for heating current 50 amps.

There is an ion current dependence on different voltages applied to deflection plates (ion current map) in picture 3.10. Ion current is measured by the Faraday cup at the end of flight tube. There could be seen how important is focusing of the beam. Both images have a similar ion current $\sim 0.7$ measured on HVPS but the largest current measured by FC on left image is 0.17 miliamps whereas on right picture it is just 0.025 miliamps. The current maximum on left image is also much more localised than the maximum on right picture due to worse focusation. This picture 3.10 shows the change of maximal current in FC due to bad focusation however this current map also changes with each replacement or assembly of the emitter. The current maximum is not in the center of the map where zero voltage is applied for this reason some offset voltages has to be applied for correct function of the beam. Deflecting plates can compensate not perfect axial setup of whole Li-beam system. The ion current map will be often used as a calibration test for experiments with Li-beam.

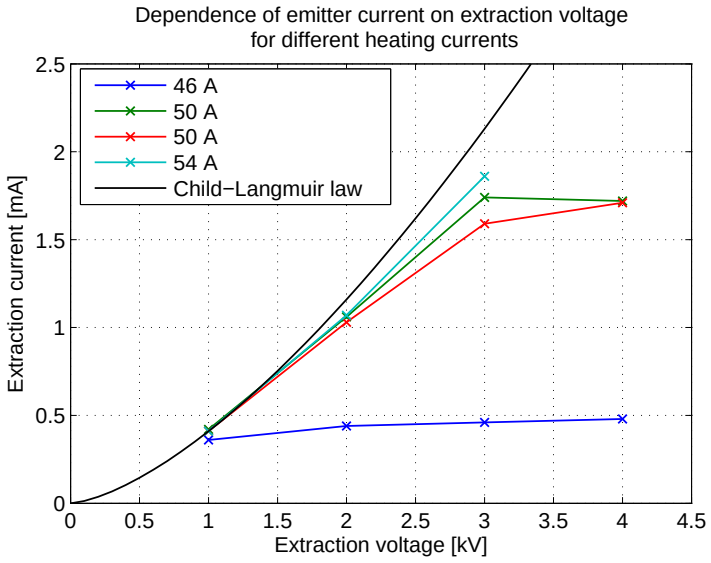


**Figure 3.9:** Measurement of extraction current.

### 3.5.2 Neutralization efficiency

There are two ways how to measure efficiency of neutralization: by the Faraday cup or by radiation in helium gas.

First the $e^-$ multiplication factor $\eta_{e^-}(E_{beam})$ of the Faraday cup for different beam energy must be obtained for measurement of neutralization efficiency with Faraday cup. This task was done by FC connection in figure 3.8. After that the neutralizer was switched on and only the FC Ti current was measured. If the housing voltage was -500 volts, electrons were suppressed and an ion current $I_{-500}$ was measured. If the housing voltage was +500 volts, electrons were pulled up by housing and the FC Ti current $I_{+500}$ consists of ion current and negative electron current produced by ion induced secondary electron emission. The current of neutral lithium atom is given by the equation

$$I_{Li^0} = \frac{I_{+500} - I_{-500}}{\eta_{e^-}(E_{beam})} - I_{-500} \tag{3.4}$$

and the neutralization efficiency is given by the formula

$$\eta_n = \frac{I_{Li^0}}{I_{Li^0} + I_{-500}} \tag{3.5}$$

Measurement of $\eta_n$ was done for different temperatures of neutralizer and different beam energy i.e. accelerating voltages. The results are shown in figure 3.11. This measurement has a few disadvantages compared to measurement with neutral gas. First the $e^-$ multiplication factor $\eta_{e^-}(E_{beam})$ has to be known with relatively low error and also the parasitic signal from $e^-$ on Faraday cup must be low. These two errors can cause a negative neutralization efficiency

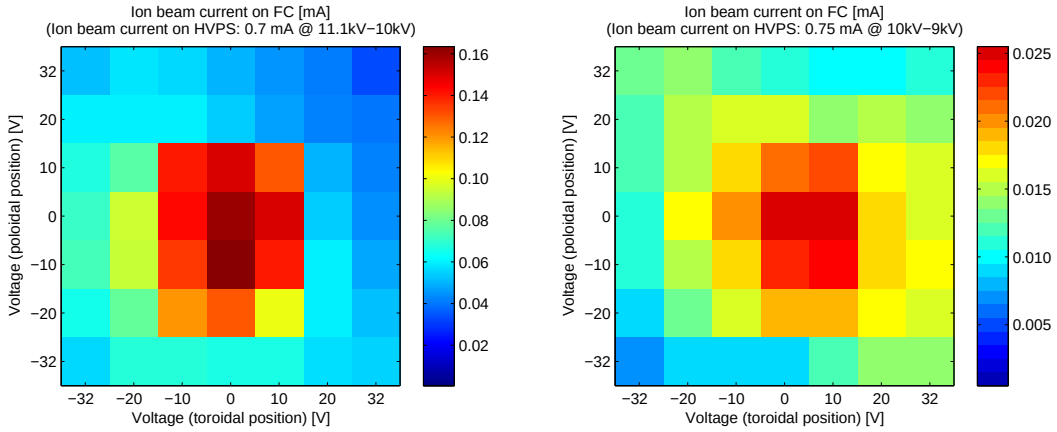


**Figure 3.10:** Ion current measured at the end of flight tube for different deflecting voltages. There can be seen difference of beam focusation in the picture.

obtained from 3.4 and 3.5 when the neutralization efficiency is low. One of the advantages of this method over the following method is that you do not need to fill a tokamak with a gas and make a tokamak not working.

The tokamak chamber is filled with helium gas and tokamak is not in operation. The gas pressure must be low considering turbomolecular pumps in Li-beam device must be able to provide optimal vacuum for operation of the Li-beam. First the neutralizer is switched off and radiation of the ion beam is captured by CCD camera then neutralizer is switched on and three magnets are placed to the flight tube in order to decline neutral particles from beam and radiation of neutral beam is captured by a CCD camera. This measurement was done for different acceleration voltages and temperatures of neutralizer. The measured data are shown in table 3.2. The ion beam receives electrons from helium gas by charge exchange and then collisional excitation and spontaneous emission cause radiation of the beam. The intensity of radiation on CCD camera pictures is proportional to the beam current.

| | shot | $\frac{U_1}{U_2}$ [kV] | $I_e xt$ [mA] | $T_{exp}$ [ms] | $\frac{T_{oven}}{T_{end}}$ [C] | $\eta$ [%] | S/N |
|---|---|---|---|---|---|---|---|
| Ion beam | #119 | 20/18 | 0.65 | 50 | | | 1.4 |
| | #122 | 30/27 | 1.78 | 50 | | | 2.5 |
| | #151 | 20/18 | 1 | 50 | | | 1.6 |
| Neutral beam | #155 | 20/18 | 0.6 | 100 | 296/140 | 54 | 1.4 |
| | #146 | 30/27 | 1.72 | 50 | 290/140 | 58 | 1.2 |
| | #145 | 20/18 | 1 | 50 | 280/140 | 64 | 1.2 |

**Table 3.2:** Measurement of neutralization efficiency from difference between radiation of ion and neutral beam detected by CCD camera.

The neutralization efficiency $\eta_n$ was around 55-65 %.

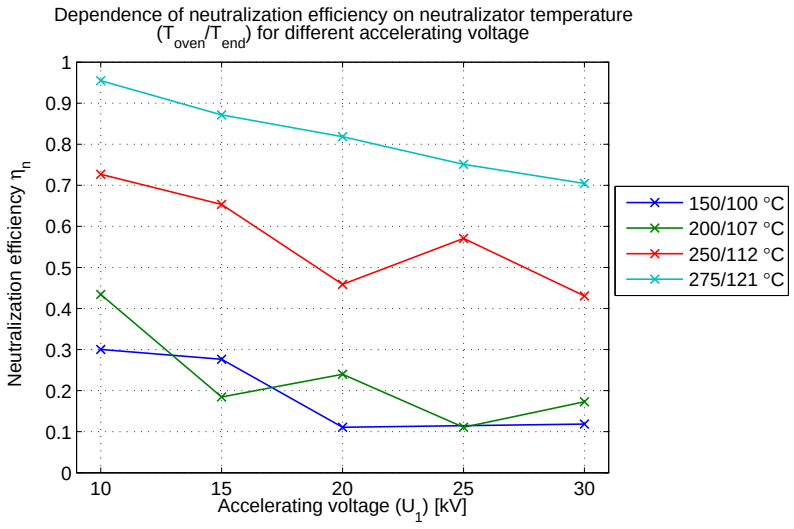


**Figure 3.11:** Neutralization efficiency for different neutralizer temperatures and acceleration voltages.

### 3.5.3 Influence of electric field

The system which control lithium beam has two grounding points in order to protect low voltage parts. First one for the parts with high voltage and the second one for the parts with low voltage and control parts. Voltages between parts with different grounding were measured and a maximal voltage was $\sim$ 1V. This is not sufficient for deflection of the beam because 150 volts has to be applied on deflection plates to fully decline the beam. The situation could change during tokamak operation considering changing poloidal magnetic field of tokamak is able to produce an extra electric field in accelerator part (thanks to different grounding). The oscilloscope measures voltage on parts with different grounding and several plasma shots were made. The results were similar during different shots. The maximal measured voltage reaches $\sim$ 3V thus the influence of the induced electric field on accelerated ion beam can be neglected.

### 3.5.4 Influence of magnetic field

There was no radiation observed with CCD camera during the shots, although there was a lithium atom current measured at the end of flight tube during previous tests. One of the reasons why the radiation is not observed is that poloidal magnetic field of the tokamak bends the trajectory of ions in HV part. The next test was to measure whether the shielding of HV part of the beam device is strong enough. There were done many tests in He gas with different setup of voltages and temperatures. The most important result is that shielding of HV part is sufficient as can be seen in picture 3.12. There could be seen the separation of ionized and neutral component of the beam when vertical magnetic field increases. This picture also gave

us an information about neutralization efficiency although an ion needs to catch an electron from a helium atom (CXRS).

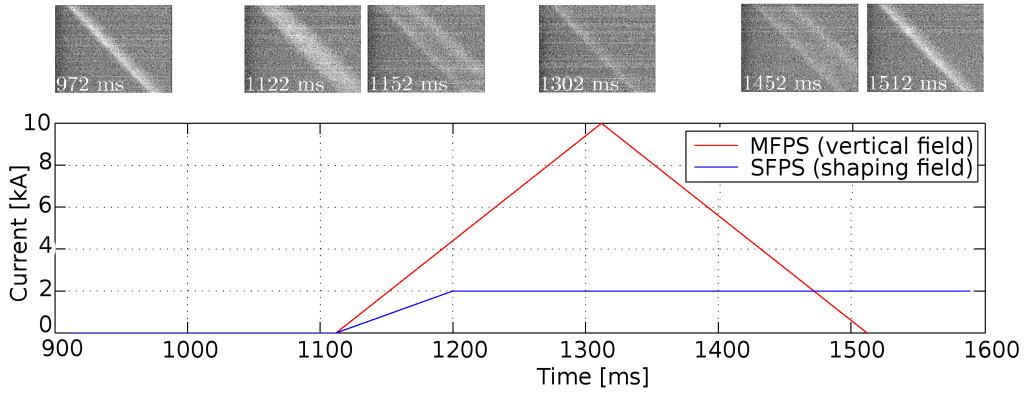


**Figure 3.12:** Top: Splitting of the beam (ion path is curved by magnetic field). Bottom: Time evolution of current in coils producing vertical magnetic field.

### 3.5.5 CCD camera

At present the CCD camera is working. The first tests were made during SUMTRAIC in 2011. The ion beam (without neutralization) injected into hydrogen gas was used during the first experiments. The magnetic coils have to be switched off for this experiment. A chamber pressure was $2{,}7{\cdot}10^{-4}$mbar. The first pictures from the CCD camera are shown in figure 3.13.

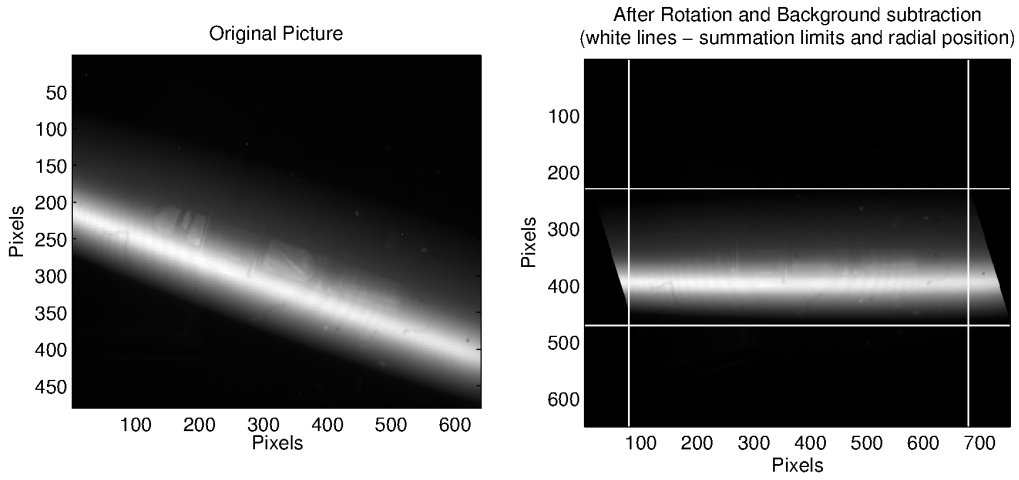


**Figure 3.13:** CCD camera picture: injection of lithium ion beam into hydrogen gas. Accelerating voltage 18 kV, emitter current 1,6 mA, exposition 1000 ms.

There is an optical filter (center wavelength 670 nm and FWHM 10 nm) in front of the

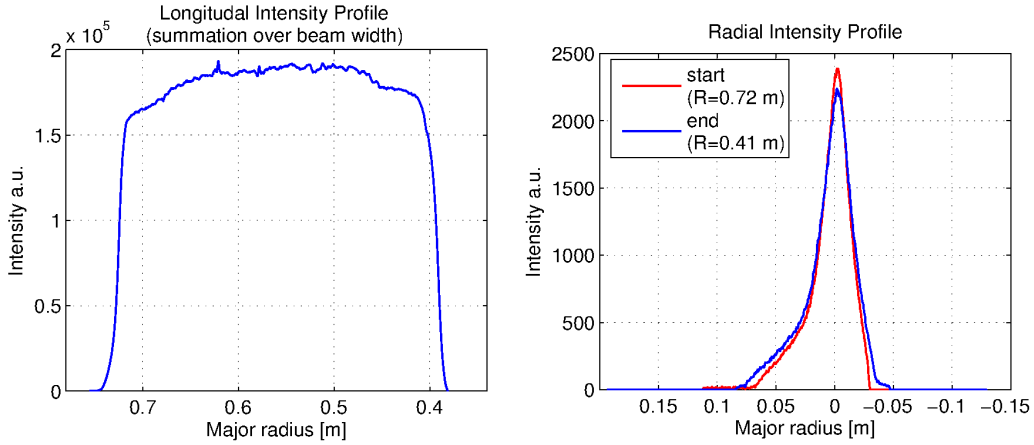


**Figure 3.14:** CCD camera picture: injection of lithium ion beam into hydrogen gas. Accelerating voltage 18 kV, emitter current 1,6 mA, exposition 1000 ms.

CCD camera. A lithium ions entering the vacuum vessel get an electron from hydrogen atoms and begin emit radiation due to collisions with hydrogen atoms. The hydrogen atoms are also excited and produce line radiation. These pictures (figure 3.13 and 3.14) can be used for getting some beam parameters although there is the $H_\alpha$ radiation captured in the picture due to high width of optic filter FWHM. Besides the light from the beam a bottom flange can be seen in the original picture. During picture transformations this background signal was subtracted using photos without the beam (same exposition time) and then the picture was rotated. The vertical section of light profile gives information about beam width and divergence. The beam divergence is relatively small and it can be neglected in numerical simulation. A steeper decrease of light signal on one side of the beam is caused by the interaction between the beam and the diaphragm in the flight tube thus the beam is cropped at one side that the reason why the diaphragms have been removed. The light profile along the beam path is constant except the edge parts where the light intensity is lower because of smaller effective solid angle of the camera. The picture can be also used for beam coordinate calibration because the position of the CCD camera and bottom flange is known.

# 4

# Beam emission spectroscopy

## 4.1 Description

Beam emission spectroscopy is an active spectroscopic method using line radiation detection of injected lithium atoms to calculate plasma electron density. This method was successfully used for 2D plasma density a density fluctuation measurement at tokamak JET [39] and also for radial density profile measurement.

## 4.2 Plasma-beam interaction

Injected lithium atoms are excited and ionized due to collision with protons and electrons in plasma. Ionized atoms are trapped by magnetic field and removed from the beam but the diagnostic method is based on detection of line radiation produced by electron transitions between energetic levels of neutral atoms. The energy levels of Li atom are shown in figure 4.1. Photons with wavelength 670.8 nm are produced by $1s^2 2s$-$1s^2 2p$ electron transition are used for measurement at tokamak COMPASS. The beam is monoenergetic and it is not in thermal equilibrium with plasma. For this reason, the interaction process is described by collisional-radiative model 4.2.1.

### 4.2.1 Collisional-Radiative model

Light intensity depends on electron populations on correspond energetic levels. A change of electron population density of the state $i$ due to collisions with electron and ions can be described by general equation [27]

$$\begin{aligned}\frac{\partial}{\partial t}n_i = &\sum_{j,j\neq i}\langle\sigma_{e,ji}v\rangle n_e n_j - \sum_{j,j\neq i}\langle\sigma_{e,ij}v\rangle n_e n_i + \sum_{j,j\neq i}\langle\sigma_{p,ji}v\rangle n_{ion} n_j - \sum_{j,j\neq i}\langle\sigma_{p,ij}v\rangle n_{ion} n_i \\ &+ \sum_{j,j>i} A_{ji} n_j - \sum_{j,j<i} A_{ij} n_i - \langle\sigma_{eion,i}v\rangle n_e n_i - \langle\sigma_{pion,i}v\rangle n_{ion} n_i - \langle\sigma_{cx,i}v\rangle n_{ion} n_i\end{aligned} \tag{4.1}$$

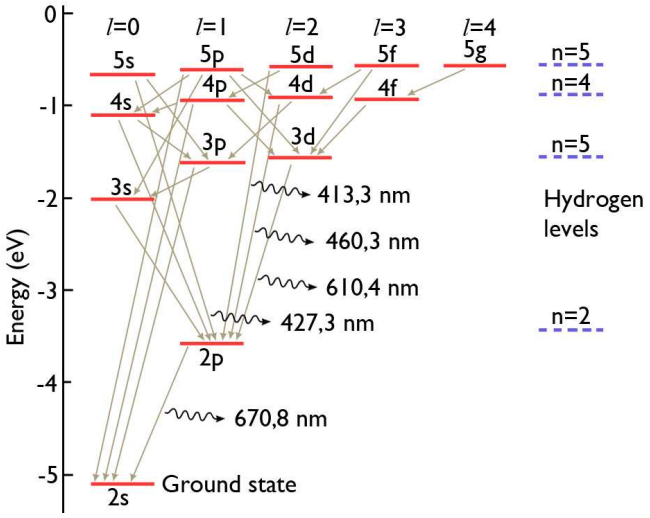


**Figure 4.1:** Lithium energy level diagram for principal quantum number $n \leq 5$. Taken from [17]

where $n_e, n_{ion}$ are electron and proton density, $n_i, n_j$ are populations of electron on i and j levels, $\langle\sigma_{e,ij}v\rangle, \langle\sigma_{p,ij}v\rangle$ are the rate coefficients for electron, resp. ion impact excitation from state i to j, $A_{ij}$ are a transition probabilities of spontaneous emission from state i to j and $\langle\sigma_{eion,i}v\rangle$, $\langle\sigma_{pion,i}v\rangle$, $\langle\sigma_{cx,i}v\rangle$ are rate coefficients for electron, resp. ion impact ionisation, resp. charge exchange.

The equation (4.1) describes time evolution of state $i$. The injected lithium atom goes across the plasma in our experiment and rate coefficients depends on the space coordinates thus dividing of the equation by the speed of lithium atom of the equation is more appropriate. When the plasma density is low then all upward transitions are primarily collisional (since the the radiation density is low) and all downward transitions are primarily radiative (since the electron density is low) [27]. The plasma is also optically thin and most photons simply escape without being absorbed thus upward radiative transitions will be negligible compared with downward [12]. The equation which describes spatial evolution of state $i$ is

$$\begin{aligned}\frac{\partial}{\partial x}n_i = \Bigg( &\sum_{j,j<i}\langle\sigma_{e,ji}v\rangle n_e n_j - \sum_{j,j>i}\langle\sigma_{e,ij}v\rangle n_e n_i + \sum_{j,j<i}\langle\sigma_{p,ji}v\rangle n_{ion} n_j - \sum_{j,j>i}\langle\sigma_{p,ij}v\rangle n_{ion} n_i \\ &+ \sum_{j,j>i} A_{ji} n_j - \sum_{j,j<i} A_{ij} n_i - \langle\sigma_{eion,i}v\rangle n_e n_i - \langle\sigma_{pEL,i}v\rangle n_{ion} n_i \Bigg) \frac{1}{v_b}\end{aligned} \tag{4.2}$$

where electron-loss cross section $\sigma_{pEL,i}$ comprises both the ionization cross section and the charge exchange cross section. It is necessary to calculate with more than just 2s and 2p levels population because a higher energetic levels affect lower energetic states. To solve this system of equations requires some simplifying assumptions because the number of equations is infinite. To truncate the system of equations at some high level is very often because the populations

of higher levels are often very small. The final system of equations is thus reduced and can be solved numerically if all appropriate coefficients are set.

### 4.2.2 Cross section

The rate coefficient represents a number of collision events per unit path length of a particle of velocity $v$ in a density $n$ of target particles. The rate coefficient can be expressed as a product of cross section $\sigma(v)$ and relative velocity of the interacting particles $v$. The rate coefficient $\sigma(v)v$ dimension is $m^3/s$. Generally the cross section also depends on the relative velocity of interacting particles. The cross section for inelastic collisions of lithium atoms with electrons, protons, and multiply charged ions can be found in database [29], [37], [6] [16]. The cross sections for appropriate processes are shown in figure 4.2 and 4.3.

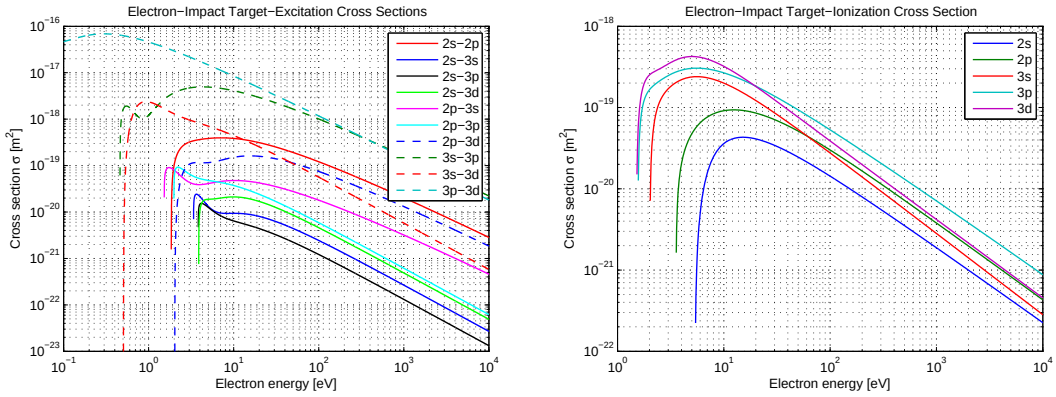


**Figure 4.2:** Cross sections for collisional processes of lithium atoms with electrons.

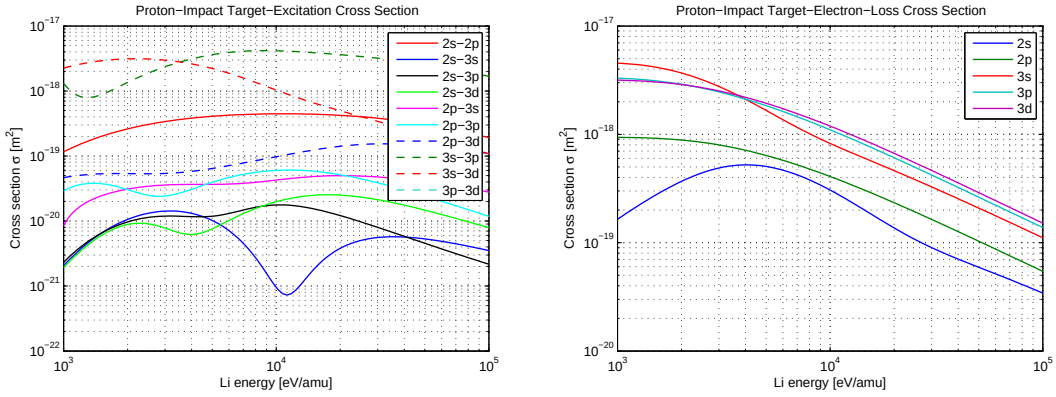


**Figure 4.3:** Cross sections for collisional processes of lithium atoms with protons.

The cross sections mentioned above was used for calculation of rate coefficients. The total rate coefficient at which the lithium atom undergoes collisions with plasma particles (electrons

or ions) is

$$\int \sigma_{ij}(|\mathbf{v_b}-\mathbf{v}|)|\mathbf{v_b}-\mathbf{v}|f(\mathbf{v})\mathrm{d}\mathbf{v} = n\langle\sigma_{ij}v\rangle \tag{4.3}$$

where $f(\mathbf{v})$ is a probability density function of plasma particles. If beam particles are much slower than plasma electrons and at the same time much faster than plasma ions (protons in hydrogen plasma) thus

$$v_p \ll v_b \ll v_e \tag{4.4}$$

(for example, $v_p$(1keV)=4.38·10$^5$ m/s, $v_b$(80keV)=1.49·10$^6$ m/s and $v_e$(1keV)=1.86·10$^7$ m/s) the equation (4.3) can be simplified as follows: (1) for ions

$$\langle\sigma_p v\rangle = \frac{\int \sigma_p(\mathbf{v_b})|\mathbf{v_b}|f(\mathbf{v})\mathrm{d}\mathbf{v}}{\int f(\mathbf{v})\mathrm{d}\mathbf{v}} = \sigma_p v_b \tag{4.5}$$

and (2) for electrons

$$\langle\sigma_e v\rangle = \frac{\int \sigma_e(\mathbf{v})|\mathbf{v}|f(\mathbf{v})\mathrm{d}\mathbf{v}}{\int f(\mathbf{v})\mathrm{d}\mathbf{v}} = \frac{\int \sigma_e(E)\sqrt{\frac{2E}{m_{\mathrm{Li}}}}f(E)\mathrm{d}E}{\int f(E)\mathrm{d}E} \tag{4.6}$$

Transformation of electron rate coefficient from the function of velocity to the function of energy is useful because cross sections are expressed as a function of energy in databases very often. There is a monoenergetic lithium beam assumed in all equations. Plasma particles are described by Maxwellian distribution

$$f(E) = 2\sqrt{\frac{E}{\pi}}\left(\frac{1}{kT}\right)\exp\left(\frac{-E}{kT}\right) \tag{4.7}$$

The equations (4.7) is put into the equation (4.6) which results in rate coefficient equation [3] for collisions with electrons

$$\langle\sigma v\rangle = \left(\frac{8kT}{\pi m_e}\right)^{1/2}\int_{E_{\mathrm{Th}}/kT}^{\infty}\sigma(E)\frac{E}{kT}\exp\left(\frac{-E}{kT}\right)\mathrm{d}\left(\frac{E}{kT}\right) \tag{4.8}$$

where $m_e$ is the electron mass, $E_{\mathrm{Th}}$ is a threshold energy for the appropriate process and $kT$ is a temperature of the plasma. Energy $E$ and temperature $kT$ are usually entered in electronvolts. The rate coefficients for appropriate processes are shown in figure 4.4. These functions were calculated by codes RCEEtable.m and RCEItable.m.

The system of the five ordinary differential equation (4.9) for 2s,2p,3s,3p and 3d level is used for numerical calculations. Inclusion of more bound Li($nl$) states $n \geq 4$ into the calculations has been tested and found to be unnecessary [30].

$$\begin{aligned}\frac{\partial}{\partial x}n_i = &\sum_{j,j<i}\frac{\langle\sigma_{e,ji}v\rangle}{v_b}n_e n_j - \sum_{j,j>i}\frac{\langle\sigma_{e,ij}v\rangle}{v_b}n_e n_i + \sum_{j,j<i}\sigma_{p,ji}n_{ion}n_j - \sum_{j,j>i}\sigma_{p,ij}n_{ion}n_i \\ &+ \sum_{j,j>i}\frac{A_{ji}}{v_b}n_j - \sum_{j,j<i}\frac{A_{ij}}{v_b}n_i - \frac{\langle\sigma_{eion,i}v\rangle}{v_b}n_e n_i - \sigma_{pEL,i}n_{ion}n_i\end{aligned} \tag{4.9}$$

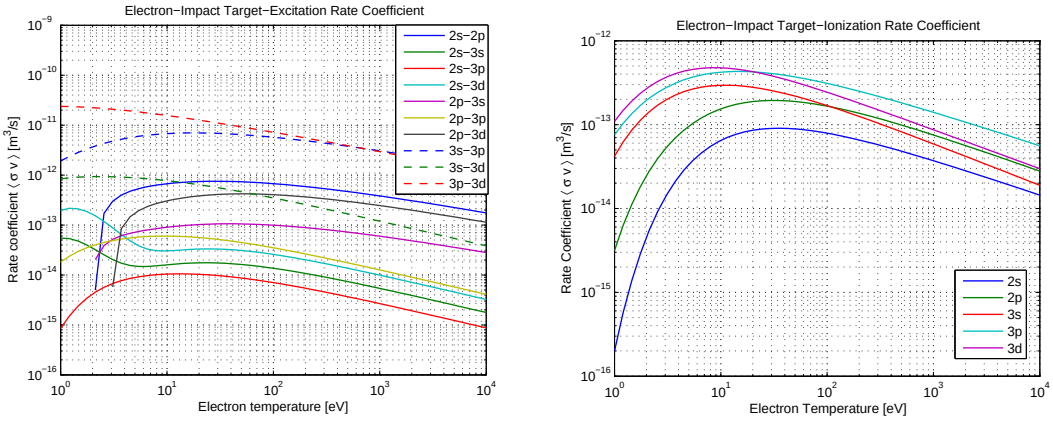


**Figure 4.4:** Rate coefficients for collisional processes of lithium atoms with electrons.

### 4.2.3 Atomic transition probabilities

Atomic transition probabilities or the Einstein coefficient for spontaneous emission represents the time at which the population of the energetic level is reduced to $1/e \approx 0.37$ times its initial value. The atomic transition probabilities for lithium atoms can be found in [36]. The emission of 2p→2s lithium line can be described by an emission coefficient $\epsilon$. It is the energy emitted by a volume element d$V$ during a time d$t$ into a solid angle d$\Omega$. For $2p \rightarrow 2s$ transition we get

$$\epsilon = \frac{h\nu}{4\pi} A_{2p\rightarrow 2s} n_{2p} \tag{4.10}$$

where $h\nu$ is the energy of the emitted photon, $A_{2p\rightarrow 2s}$ is the Einstein coefficient for spontaneous emission between 2p and 2s levels and $n_{2p}$ is the number of atoms with electrons in the 2p energetic state.

## 4.3 Optics

### 4.3.1 Doppler shift

The velocity of the lithium atoms is in range 7.5 - 14.9·10$^5$ m/s for the energy in range 20 - 80 keV. Doppler shift can be expressed by following equation:

$$\Delta\lambda = \lambda \frac{v_b \cos\alpha}{c} \tag{4.11}$$

where $\lambda$ is a wavelength of observed radiation, $v_b$ is a beam velocity, $\sin\alpha$ is the angle between line of sight and a beam and $c$ is a speed of light. The observation angle of the beam is 60 degrees in the edge plasma region and 90 degrees in the plasma center. The Doppler shift for these angles is 1.7 nm in the edge plasma region and zero shift in the center if the velocity 14.9·10$^5$ m/s is assumed. Due to the fact that the FWHM of optical filter is 10 nm at center wavelength 670 nm a Doppler shift will have no influence on the detected signal. The impact of Doppler broadening on detected light can be also neglected because the beam has extremely

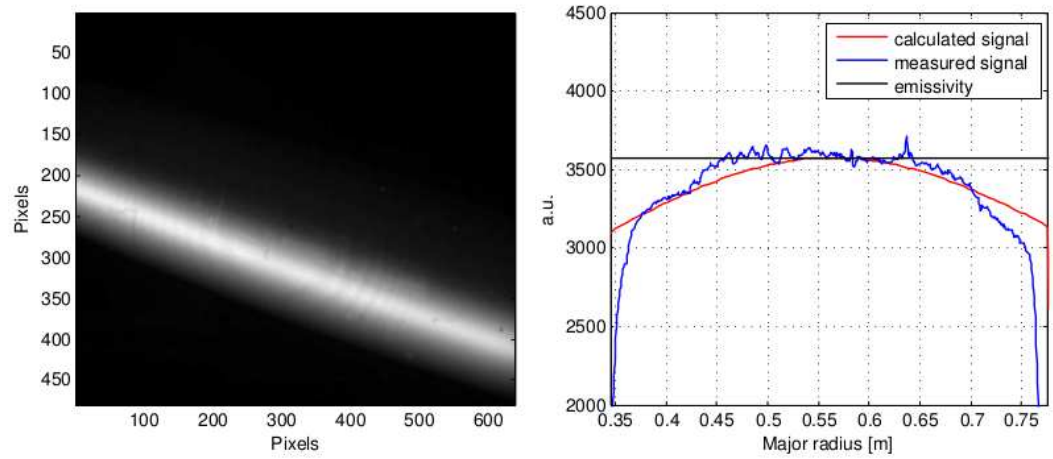


**Figure 4.5:** Left: Picture of lithium ions interacting with hydrogen gas (without background signal). Right: Measured light profile compared with the calculated light profile (constant photon intensity flux is assumed).

narrow velocity distribution both in direction perpednicular to the beam and in the direction of the flight.

### 4.3.2 Light intensity

The plasma is optically thin for measured wavelength. It means that photons simply escape without being reabsorbed. The intensity of radiation from volume element $\mathrm{d}V$ during a time $\mathrm{d}t$ into a solid angle $\mathrm{d}\Omega$

$$\mathrm{d}I = \epsilon \mathrm{d}V \mathrm{d}t \mathrm{d}\Omega \tag{4.12}$$

The solid angle from which a volume element of beam $\mathrm{d}V$ is seen depends on distance $\vec{R}$ between the lens and volume element and surface $\vec{S}$ of the lens by formula

$$\mathrm{d}\Omega = \frac{\vec{R}S}{R^3} = \frac{S\cos\alpha}{R^2} \tag{4.13}$$

If the curvature of the lens is neglected and replace by plane with surface $S$ because of small $\alpha$ the final formula for solid angle is

$$\mathrm{d}\Omega = \frac{S\cos\beta}{R^2} \tag{4.14}$$

where $\beta$ is the angle between line of sight and beam path and $S\cos\beta$ represents an effective area of the lens. The formulas 4.14 and 4.12 give us an equation for radiation intensity from volume element $\mathrm{d}V$ in time interval $\mathrm{d}t$

$$\mathrm{d}I = \epsilon \frac{S\cos\beta}{R^2} \mathrm{d}V \mathrm{d}t \tag{4.15}$$

which is used for simulation. This formula was tested on data during experiments with hydrogen gas in tokamak chamber (see figure 4.5). The emissivity of the beam is almost same in

whole chamber because the lithium ions reach an equilibrium state with hydrogen atoms in the entrance of the chamber and then the conditions do not change. There is an original camera photo and the intensity profile compared with the calculated profile based on a formula 4.15 in figure 4.5.

# 5

# Density reconstruction

## 5.1 Principles

The aim of reconstruction is to obtain density profile from 2p→ 2s transition radiation profile. A several approaches can be used for density reconstruction from Li I (2s-2p) emission profiles.

The conventional method [30] is based on an algebraic rearrangement of the differential equation 5.1 for the 2p level obtaining an explicit equation for the density $n_e$ as a function of the beam coordinate $z$ and of all occupation densities. Density profile is obtained by stepwise integration starting at $z = 0$.

The statistical approach [11] uses Bayesian probability theory (BPT). It is based on a probabilistic description of measured data and forward calculation of emission profile from a given density profile. In comparison with conventional method, the probabilistic method main advantage is an estimation of density error.

A proposed method uses forward run to calculate the radiation profile from density profile and backward run for estimation of density profile based on minimization of calculated and measured radiation profile. Collisional and radiation processes of lithium beam in tokamak plasma are described by a system of equation 5.1. A system of equation 5.1 is solved by common fourth-order Runge–Kutta method and minimization is done by functions implemented in Matlab (Optimization Toolbox [21]). The whole code is written in Matlab environment.

## 5.2 Program structure

A schematic drawing of program structure can be seen in figure 5.1. Main loop of the code iteratively reconstruct plasma density. It consist of Runge-Kutta solver for ODE system, optical code which takes into account effect of optical apparatus, comparator which quantitatively evaluate the difference between measured and calculated light signal and optimization toolbox which changes plasma density. The cycle runs until the stopping criteria are fulfilled. Rate coefficients and cross sections for RK solver are loaded from pre-calculated tables to save computing time.

A diagnostic is not absolutely calibrated because of two major reasons. Although variation of light profile with electron temperature is low, some temperature profile has to be used for calculation. A data from Thomson scattering diagnostic or interferometry diagnostic can be used in case of COMPASS tokamak. The optical apparatus is not calibrated thus calculated density profile has to be calibrated from Thomson scattering diagnostic or the CCD camera has to be calibrated by radiometrically calibrated light source. The last way to solve problem with optical apparatus is to implement ABSOLUT code [28] which can absolutely calibrate the density profile from the relative light profile if the attenuation of light profile due to dominant ionization process is seen.

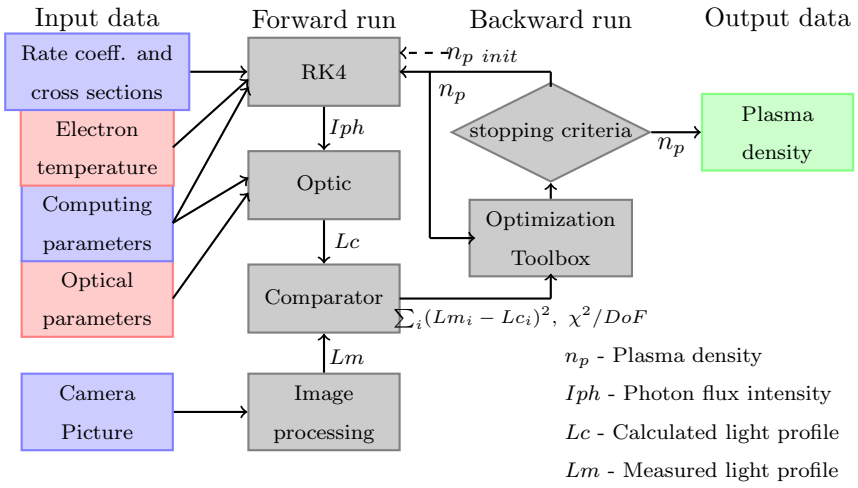


**Figure 5.1:** Program structure

## 5.3 Light profile calculation (forward run)

The density of photon flux intensity [9] (number of photons detected per solid angle per second produced in cubic meter) was calculated by Runge-Kutta method. The input data are plasma density $n_p$ ($Z_{\text{eff}} = 1$) and electron temperature $T_{\text{e}}$. The photon flux intensity profile for different beam energy and the population of Li states are shown in figure 5.2.

The photon intensity is proportional to 2p excitation state which is mostly populated. The decrease of ionization cross section for higher beam energies causes a greater range of beam atoms. Optical code calculates solid angle and observed volume of beam for each pixel and multiplies it with corresponding photon intensity thus computed profile can be compared with measured.

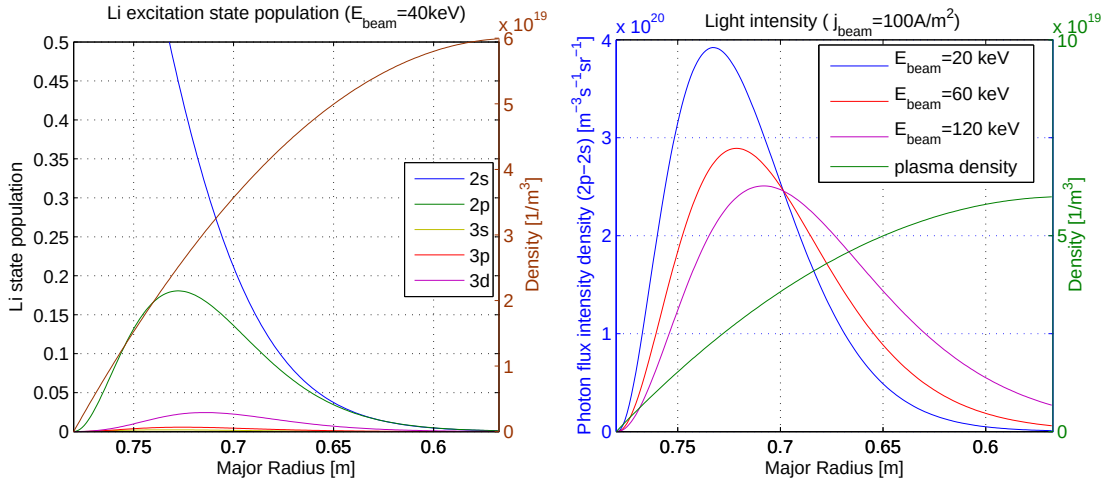


**Figure 5.2:** Results of forward run for parabolic density profile. Left: Calculated Li state population profiles for beam energy 40 keV. Right: Calculated photon flux intensity profiles for different beam energy.

### 5.3.1 Runge-Kutta method

Rewriting of the equation system

$$\begin{aligned}\frac{\partial}{\partial x}n_i = &\sum_{j,j<i}\frac{\langle\sigma_{e,ji}v\rangle}{v_b}n_e n_j - \sum_{j,j>i}\frac{\langle\sigma_{e,ij}v\rangle}{v_b}n_e n_i + \sum_{j,j<i}\sigma_{p,ji}n_{ion}n_j - \sum_{j,j>i}\sigma_{p,ij}n_{ion}n_i \\ &+ \sum_{j,j>i}\frac{A_{ji}}{v_b}n_j - \sum_{j,j<i}\frac{A_{ij}}{v_b}n_i - \frac{\langle\sigma_{eion,i}v\rangle}{v_b}n_e n_i - \sigma_{pEL,i}n_{ion}n_i\end{aligned} \tag{5.1}$$

for $i \in \{1,2,3,4,5\}$ (2s,2p,3s,3p and 3d level) to formula

$$\frac{\mathrm{d}}{\mathrm{d}x}\vec{n}(x) = \mathbf{F}(x, E_{beam})\vec{n}(x) \tag{5.2}$$

where $\vec{n}$ is a density vector of Li atoms in correspond states and $\mathbf{F}(x, E_{beam})$ is $5 \times 5$ matrix which is function of $x$ and beam energy $E_{beam}$ is useful for numerical method description. A discretization of coordinate $x$ with step $h$ creates an $n$ point uniform computational grid $x_i$ for $i \in \{1, 2, \ldots, n-1\}$ . If $\vec{n}_i$ denotes a density in point $x_i$ than a density $\vec{n}_{i+1}$ calculated by the RK4 method is given by equations

$$\begin{aligned}\vec{n}_{i+1} &= \vec{n}_i + \frac{1}{6}(\vec{k}_1 + 2\vec{k}_2 + 2\vec{k}_3 + \vec{k}_4) \\ x_{i+1} &= x_i + h \\ \vec{k}_1 &= h\mathbf{F}(x_i, E_{beam})\vec{n}_i \\ \vec{k}_2 &= h\mathbf{F}(x_i + \frac{h}{2}, E_{beam})(\vec{n}_i + \frac{1}{2}\vec{k}_1) \\ \vec{k}_3 &= h\mathbf{F}(x_i + \frac{h}{2}, E_{beam})(\vec{n}_i + \frac{1}{2}\vec{k}_2) \\ \vec{k}_4 &= h\mathbf{F}(x_i + h, E_{beam})(\vec{n}_i + \vec{k}_3)\end{aligned} \tag{5.3}$$

with initial condition $\vec{n_0}$ in point $x_0$ which correspond to density of Li atoms in different excitation states before the entrance to the tokamak chamber. The step was set with respect to relative error of solution. The ODE system with different density profile, and beam energy was calculated by `ode45` matlab function with required relative error 0.1% and after that the minimal step of all runs was used for calculation with proposed code. This approach secures maximal relative error 0.1% and it is 10 times faster than `ode45` solver.

## 5.4 Density reconstruction (reverse run)

Main input data in reverse run are measured light profile $Lm$ and calculated light profiles $Lc(n_p)$ from which plasma density $n_p$ is reconstructed. At the beginning of reconstruction a random density profile is created and used for light profile calculation. This profile is compared with the measured light profile and sum of squared residuals is obtained (residuals are the difference between signals) i.e. the maximum likelihood method [8] is used for finding density profile. Then two ways of density reconstruction are used for light signal but for both a Matlab optimization toolbox is used, especially solvers for nonlinear least squares and constrained problems.

### 5.4.1 Method of maximum likelihood

Consider a random variable $x$ distributed according to a probability density function (PDF) $f(x;\theta)$. Suppose the functional form of $f(x;\theta)$ is known, but the value of parameter $\theta$ are not known. The method of maximum likelihood is technique for estimating parameter $\theta$ when a finite sample of data is given. Suppose $x_1,\ldots,x_n$ is measurement of variable $x$ repeated $n$ times. Under the assumption of the hyphothesis $f(x;\theta)$, the probability of the first measurement to be in inerval $(x_1, x_1+\mathrm{d}x_1)$ is $f(x_1;\theta)\mathrm{d}x_1$. Since the measurements are all assumed independent, the probability that $x_i \in (x_i, x_i+\mathrm{d}x_i)$ for all $i$ is given by

$$\prod_{i=1}^{n} f(x_i;\theta)\mathrm{d}x_i \tag{5.4}$$

If the hyphothesized PDF and parameter values are correct, one expects a hight probability for the data that were actually measured and since the $\mathrm{d}x_i$ do not depend on parameters $\theta$, the same reasoning also applies to the following function L,

$$L(\theta) = \prod_{i=1}^{n} f(x_i;\theta) \tag{5.5}$$

called the likelihood function. The maximul likelihood estimators for the parameters will be those which maximize the likelihood function 5.5 thus the estimators are given by the solutions to the equations,

$$\frac{\partial L}{\partial \theta_i} = 0, \quad i = 1,\ldots,m. \tag{5.6}$$

In case of light detection the measured value $Lm$ can be regarded as a Gaussian random variable centered about the quantity's true value $L$. This follows from the central limit theorem.

Consider a set of N independent Gaussian random variables $Lm_i$, $i = 1, \ldots, N$, each related to coordinate $x_i$, which is assumed to be known without error. Assume that each value $Lm_i$ has a different unknown mean $L_i$ and a different but known variance $\sigma^2$. The N measurements of $Lm_i$ can be equivalently regarded as a single meausurement of an N-dimensional random vector, for which a joint p.d.f. is the product of N Gaussians,

$$g(Lm_1, \ldots, Lm_N; L_1, \ldots, L_N; \sigma_1^2, \ldots, \sigma_N^2) = \prod_{i=1}^{N} \frac{1}{\sqrt{2\pi\sigma_i^2}} \exp\left(\frac{-(Lm_i - L_i)^2}{2\sigma_i^2}\right) \tag{5.7}$$

Suppose further that true value is given as a function of $x$, $L = L(x; \vec{n_p})$, which depends on plasma density $\vec{n_p}$. The aim of the method of least squares is to estimate the plasma density $\vec{n_p}$. Taking the logarithm of the joint p.d.f. and dropping additive terms that do not depend on the plasma density gives log-likelihood function,

$$\log L(\vec{n_p}) = -\frac{1}{2} \sum_{i=1}^{N} \frac{(Lm_i - L(x_i; \vec{n_p}))^2}{\sigma_i^2} \tag{5.8}$$

This is maximized by finding the values of the plasma density $n_p$ that minimize the quantity

$$\chi^2(\vec{n_p}) = \sum_{i=1}^{N} \frac{(Lm_i - L(x_i; \vec{n_p}))^2}{\sigma_i^2} \tag{5.9}$$

namely quadratic sum of the differences between measured and hypothesized values, weighed by the inverse of variances.

### 5.4.2 Measurement error

There are two species of noise in the experiment - photon noise and detector-generated noise.

Photon noise consists of noise due to signal radiation and noise due to background radiation. If the ideal, noiseless detector is assumed then detection of photons is affected by radiation noise [9]. It follows from the fact that photon production is a random process. It will be assumed that the photon-emission process follows a Poisson distribution. The probability of $n$ photons being emitted in a period of time $T$ can be estimated using the Poisson PDF [23]:

$$P_T(n) = \frac{\bar{n}^n}{n! \mathrm{e}^{\bar{n}}} \tag{5.10}$$

where $\bar{n}$ is the average number of photons emitted in a period of length $T$. The probability of detection of $m$ photons in a period $T$ with perfect quantum efficiency is given by PDF:

$$P_T(m) = \frac{\bar{n}^m}{m! \mathrm{e}^{\bar{n}}} \tag{5.11}$$

The fact that there is noise (uncertainty in magnitude) present in the signal implies a limit to the signal-to-noise ratio attainable in perfect, noiseless detector. Due to the fact that the variance of a Poisson distribution is equal to the mean

$$\sigma_{var}^2 = \bar{n} \tag{5.12}$$

the root mean square noise level is defined to be the square root of variance:

$$\sigma = \sqrt{\bar{n}} \tag{5.13}$$

The photon noise affects measurement with signal radiation noise $\sigma_{sig}$ and background radiation noise $\sigma_{bg}$. The previous error does not depend on the properities of the detector. There is a wide range of detector noises [9] but in this case global marking electron noise will be sufficient. The main influence on electron noise has a temperature of the camera. The detector error $\sigma_{det}$ were estimated from dark picture. A root mean square of all mentioned errors

$$\sigma_l = \sqrt{\sigma_{sig}^2 + \sigma_{bg}^2 + \sigma_{det}^2} \tag{5.14}$$

represent the error of measured light profile .

### 5.4.3 Goodness-of-fit testing

The $\chi^2$ value can be used as a test of how likely it is that the hypothesis, if true, would yield the observed data. The quantity $(Lm_i - L(x_i; \vec{n_p}))/\sigma_i^2$ is a measure of the deviation between $i$th measurement $Lm_i$ and the function $L(x_i; \vec{n_p})$, so $\chi^2$ is a measure of total agreement between observed data and hypothesis. It can be shown [8] that if

1. the $Lm_i$ for $i = 1, \ldots, N$ are independent Gausssian random variables with known variances $\sigma_i^2$,
2. the hypothesis $L(x; \vec{n_p})$ is linear in the parameter $\vec{n_p}$ and
3. the function form of the hypothesis is correct,

then the minimum value of $\chi^2$ defined by equation 5.9 is distributed according to the $\chi^2$ distribution with $N - m$ degrees of freedom (DoF). So the $\chi^2$ divided by the number of degrees of freedom $n_d$ (number of data points minus the number of independent parameters) is a measure of goodness-of-fit. If it is much less than one, then fit is better than expected given the size of measurement errors. It is usually grounds to check that errors $\sigma_i$ have not been overestimated or are not correlated. If $\chi^2/n_d$ is much larger than one, then there is some reason to doubt the hypothesis.

### 5.4.4 Smoothed signal

If the real data are smooth or the algorithm is tested by a calculated signal then a light profile is without noise. In this case the minimizing function is the sum of squared residuals thus it is same as the method of least squares with maximum likelihood estimation.

$$\min_{\vec{n_p} \in \langle \vec{lb}, \vec{ub} \rangle} \sum_i (Lm_i - Lc(\vec{n_p})_i)^2 \tag{5.15}$$

where $lb$ and $ub$ are lower and upper bound. The boundaries are given by physical constraints of tokamak plasma. The calculation is stopped when the change of minimizing function in the last step is lower than function tolerance TolFun.

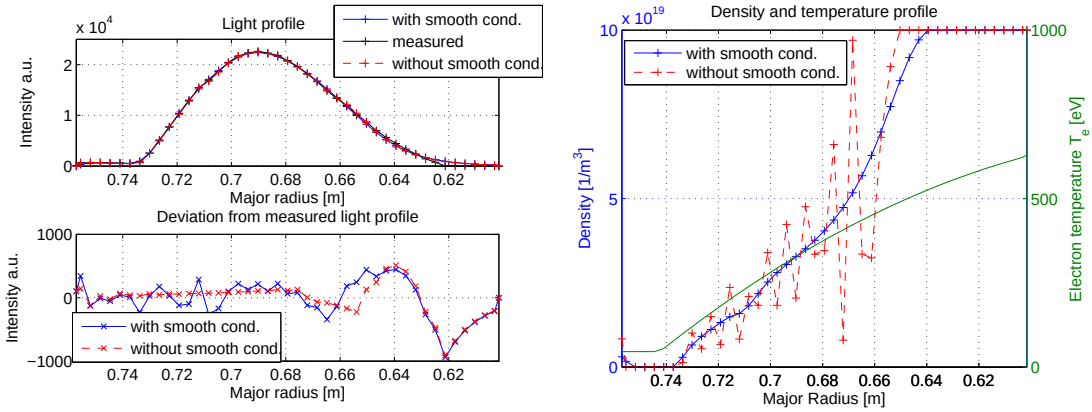


**Figure 5.3:** Impact of condition for smooth density profile. The oscillations of density profile are the result of ill-conditionality of reconstruction model.

### 5.4.5 Noisy signal

Reconstruction of the noisy light profile using the method of least squares connected with maximum likelihood produce an unreal plasma density profile because noise is much more fitted than the true values. For this reason smooth profile condition has been added to the reconstruction algorithm to prevent jumps in density. It is shown in figure 5.3 that minimization of the sum of squared residuals + the first derivative of density help to solve the problem. The algorithm for reconstruction could be written in the form:

$$\min_{\vec{n_p} \in \langle \vec{lb}, \vec{ub} \rangle} \left( \sum_i (Lm_i - Lc(\vec{n_p})_i)^2 + \lambda \frac{\mathrm{d}\vec{n_p}}{\mathrm{d}x} \right) \tag{5.16}$$

where lagrange multiplier $\lambda$ is chosen to satisfy $\frac{\chi^2}{DoF} \sim 1$.

The additional condition also helps when integration step for light profile is small. It can be seen in figure 5.3. There are reconstructed density profiles with and without the condition on smooth density profile.

## 5.5 COMPASS data

### 5.5.1 Image processing

A measurement consists of two consecutive pictures, picture with the beam in plasma and the picture with decline beam which serves for background signal measurement. After subtraction of pictures and integration of signal over the beam width a 1D lithium emission profile is obtained. A minimal exposition time of the CCD camera is 20 ms and sets up a temporal resolution of diagnostic if the impact of density changes on background signal is negligible if not then temporal resolution is 2 times longer. For this reason, the CCD camera is much more suitable for flattop phase measurement. The image processing of shot #4163 is shown if figure 5.4. It is only useable picture from COMPASS on accoung of problems with cropping of signal

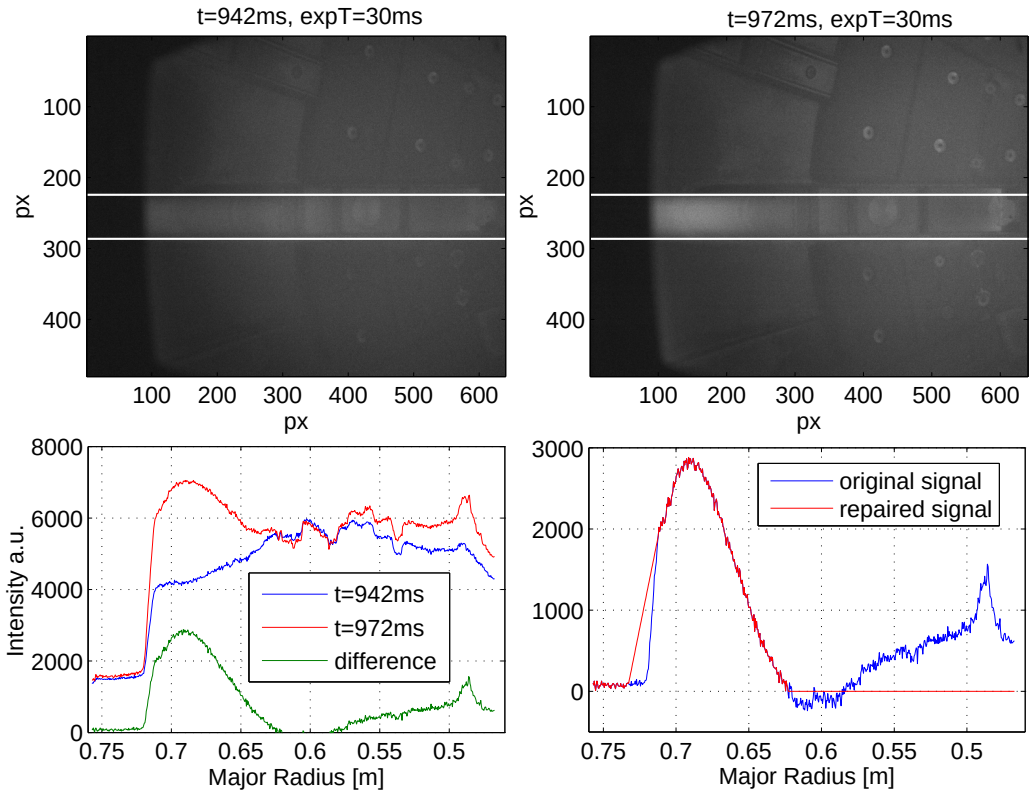


**Figure 5.4:** Image processing of the signal in shot #4163. White lines represent integration limits.

(bad camera position) and background subtraction (no background signal picture) consequently the picture was repaired as follows:

1. The previous picture was used as background signal by reason of low plasma density and low Li-beam signal.

2. LCFS was found from EFIT in time t=985ms and missing signal was completed with linear interpolation between last measured signal and LCFS point.

### 5.5.2 Density reconstruction

A data from the shot #4163 were used for reconstruction. Central electron temperature was taken from TS in shot #4162 in t=1005 ms (similar density as in shot #4163 in t=985 ms). It can be shown 5.5.3 that accuracy of temperature profile estimation has not crucial importance for the diagnostic. The reconstructed density profile which is not calibrated is shown in figure 5.5. The measured light profile and light profile calculated form reconstructed density is also show in figure 5.5. The density profile is not calibrated.

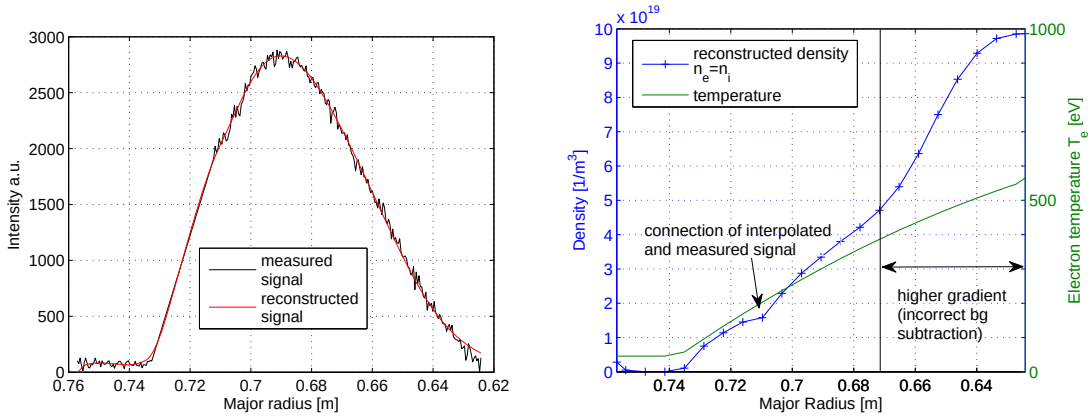


**Figure 5.5:** Right: Reconstructed density profile in shot #4163. The density profile is not calibrated. Left: Measured light profile and light profile calculated from reconstructed density profile.

### 5.5.3 $T_e$ influence on reconstruction

The electron temperature profile cannot be estimated from Li-beam measurement and must be inserted to the simulation from other diagnostic. This fact might reduce self-sufficiency of diagnostic if the effect of electron temperature on density profile was significant. For this reason a different parabolic temperature profiles were used for recontruction to measured signal in shot #4163. The influence of electron temperature profile $T_e$ on reconstructed density profile is shown in figure 5.6.

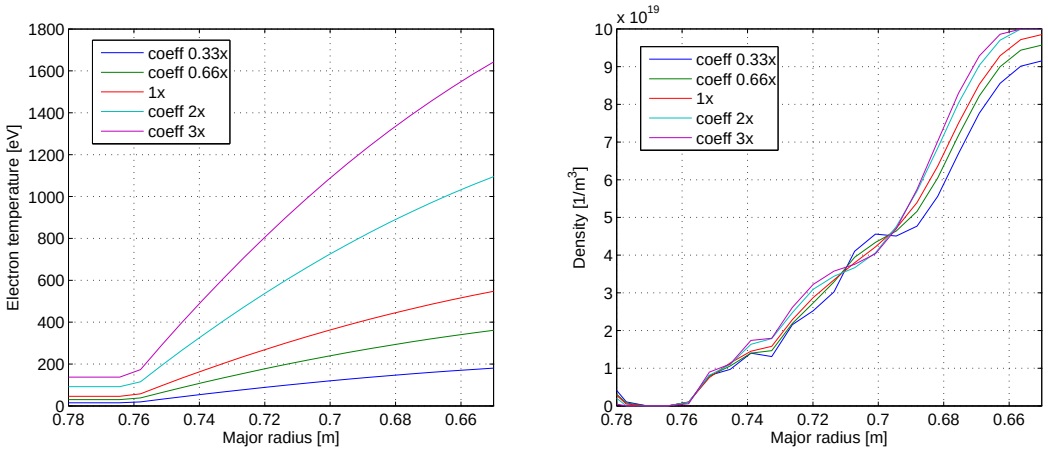


**Figure 5.6:** The influence of different electron temperature profiles (left) to density reconstruction (right). A correct temperature is shown with red line.

There could be seen that the change of central electron temperature in range 33% - 300%

of correct temperature causes changes in the density profile in range 86% - 120% of the correct density profile. If the temperature error will be 40% then the error of density profile will be less than 5%. This result shows that temperature profile estimation is not crucial for Li-beam diagnostic of the plasma in ohmic regime.

### 5.5.4 Density uncertainty

There is no method for estimating density error for this reconstruction method. For this reason rough estimation of error propagation was developed giving a basic information about density uncertainty. The light profile function can be written as

$$L = f(n_e(z), T_e(z), \alpha(z)) \tag{5.17}$$

where $f$ is a function of electron density $n_\mathrm{e}$, temperature $T_\mathrm{e}$ and parameter $\alpha$ comprising effective charge $Z_\mathrm{eff}$, beam energy $E_\mathrm{beam}$ etc. and the $z$ are the coordinates of the beam. Considering negligible importance of $\alpha$ in density error estimation, the error propagation formula [18] for light profile is

$$\sigma_L^2(z) = \left(\frac{\partial f}{\partial n_\mathrm{e}}\right)^2 \sigma_{n_\mathrm{e}}^2(z) + \left(\frac{\partial f}{\partial T_\mathrm{e}}\right)^2 \sigma_{T_\mathrm{e}}^2(z) \tag{5.18}$$

if $n_\mathrm{e}$ and $T_\mathrm{e}$ are independent. The second term of right hand side is much more smaller than the first one (see 5.5.3) thus the equation 5.18 simplifies to the form

$$\sigma_L^2(z) = \left(\frac{\partial f}{\partial n_\mathrm{e}}\right)^2 \sigma_{n_\mathrm{e}}^2(z) \tag{5.19}$$

The first derivative of $f$ with respect to $n_\mathrm{e}$ is not calculated locally in point $z$ but globally. It means the whole density profile is changed. The goal of this method is to take non-local character of excitation and spontaneous emission into account.

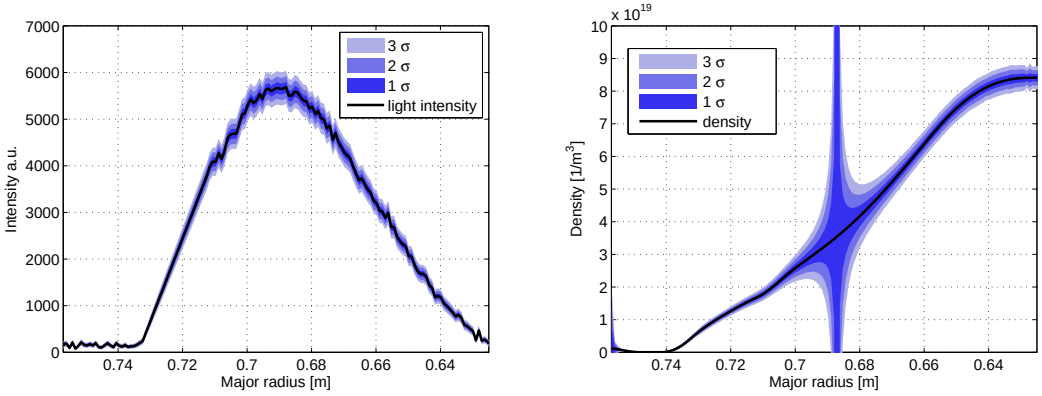


**Figure 5.7:** Left: Error of light profile. Right: Calculated density error. The maximum error in the centre represents the point around which the light profile "rotates" when the density changes.

The function $f$ is represented by a system of equation 5.1 and it is realised by numerical simulation accordingly the derivatives are calculated numerically. The density uncertainty is given by

$$\sigma^2_{n_e}(z) = \frac{1}{\left(\frac{\partial f}{\partial n_e}\right)^2}\sigma^2_L(z) \tag{5.20}$$

The result density uncertainties based on this model are shown in figure 5.7.

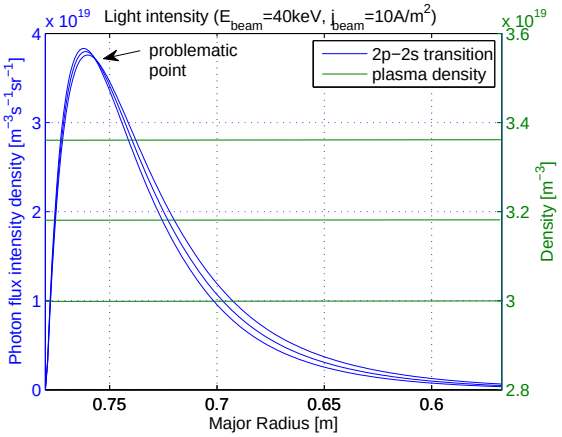


**Figure 5.8:** Light profiles for different flat density profiles. The arrow shows a point in which a small change in density profile has no influence on light intensity.

The error is increasing from the beginning of the beam path to the end except one point which has infinite error. This growing error behaviour correspond to the error propagation in light profile. The problematic point has an infinite error. The infinite error in light profile occurs when the first derivative of light profile with respect to density profile is equal to zero. The behaviour of light profile for small density changes can be seen in figure 5.8.

## 5.6 TEXTOR data

The program was tested on old data from TEXTOR tokamak to prove that program reconstruction can distinguish between H-mode and L-mode. The shot #112738 was suitable for this test. The parameters of shot are summarised in table 5.1.

| | | | |
|---|---|---|---|
| Plasma gas | deuterium | NBI1 gas | hydrogen |
| Magnetic field | 1.3 T | NBI1 start | 1s |
| Plasma density | $2.1{\cdot}10^{19}$ m$^{-3}$ | NBI1 stop | 5s |
| Plasma current | 230 kA | | |

**Table 5.1:** Basic parameters of TEXTOR shot #112738.

The central temperature was estimated to 1keV and parabolic profile was used for reconstruction. The reconstructed density profile in shot #112738 si shown in figure 5.9.

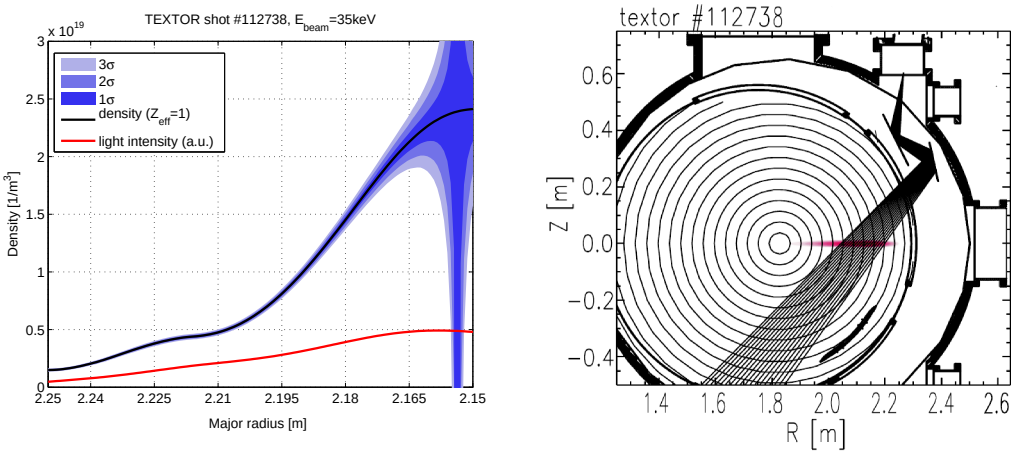


**Figure 5.9:** Left: Reconstructed density profile. The density profile is not absolutely calibrated. Right: Experimental setup [24].

The optic parameters were roughly estimated from the experimental setup (see figure 5.9). The 0s-1s and the 1s-5s reconstructed density profiles were averaged and increase in density gradient can be seen 5.10.

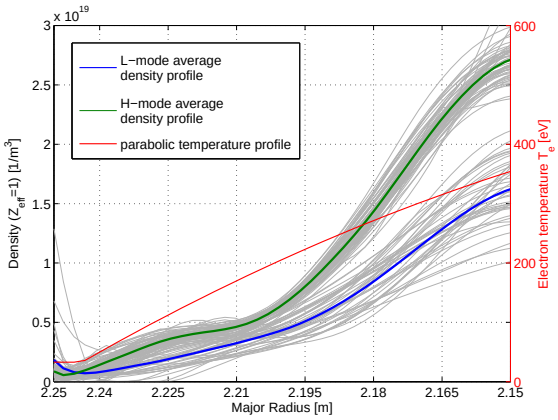


**Figure 5.10:** Reconstructed density profiles. The density profiles are not absolutely calibrated.

There is clearly seen the difference between density profiles in L-mode and H-mode. The density is not absolutely calibrated because the central density has to be about $2.1 \cdot 10^{19}$ m$^{-3}$ see table 5.1.

# 6

# Discussion

The theoretical part of this master theses work deals with the description of Li-beam diagnostic system and Beam Emission Spectroscopy. The BES measurement technique and plasma density reconstruction method are fully described in chapters 4 and 5 and furthermore they are supplemented by information about experimental setup and beam device in chapter 3. I developed a new code for density reconstruction in the MATLAB environment. The creation of this code also fulfilled a requirement of having own and fast enough reconstruction code on COMPASS tokamak. The key element of code development was the testing of the code. A typical picture from COMPASS tokamak was not available during a major part of a programming time. Due to this fact I spent a lot of time by testing a code with simulated signal. This approach is not only less effective than use of real data but also does not allow comparison with other diagnostics. While I was not developing the code I participated in the beam testing and installation with Hungarian colleagues.

The core of the proposed code is solver for Collisional-Radiative model which is enhanced by optimization toolbox. The optimization toolbox helps to find density profile which corresponds to measured light profile if the light profile was calibrated. If not, then it must be multiplied by calibration constant. In our case a calibration constant was roughly estimated by optimization toolbox (the correct constant minimizes a residuals between measured an calculated signal) but the ABSOLUTE code find these constant by much more sophisticated way. This is good reason to implement ABSOLUTE code in future. My effort was to estimate an error of the reconstructed density profile, but an error estimation method for this kind of reconstruction does not exist in present days. For this reason I have tried a several ways how to estimate an error on the base of instructions of Miklós Berta. This effort resulted in rough error estimation method described in chapter 5. The different approach is to use a Bayesian probabilistic theory but it cannot be used for my reconstruction method so far.

The practical part of theses deals with beam testing and plasma density reconstruction on tokamak COMPASS and TEXTOR. The main beam parameters and behaviour of the beam device were verified during the testing phase. The results from testing are summarized in chapter 3. A behaviour of ion optic and neutralizer was tested by Faraday cup. After these conventional tests the Li-beam was not seen in plasma during the shot therefore the next tests

with electric and magnetic field were done. However the reason why the beam did not work during a shot has not been sufficiently answered yet. The testing shows that the tokamak stray field has a crucial importantce in beam operation in negative way therefore a low number of successful measurements were done during plasma discharge on COMPASS. The 3 plasma discharges with a Li-beam observed in plasma were done. The shot #4163 was suitable for a density reconstruction and test of the algorithm. This is the reason why old data from TEXTOR tokamak were used for code testing. The analysis of reconstructed density on TEXTOR resulted in successful distinction between H-mode and L-mode regimes. Which confirmed that the reconstruction process seems correct.

Despite that the lack of data caused that the reconstructed profiles was never directly compared with different diagnostic method such as Thomson scattering or microwave reflectometry which could confirm or disprove the correct operation of code. The uncropped measurement with beam chopping was not realized because the Li-beam device was not correctly operating until the deadline of this thesis.

In conclusion, the next step will be to distinguish between H-mode and L-mode regimes on COMPASS tokamak despite the reconstructed profiles are not calibrated. The another CCD pictures with background signal measurement would improve the code as well as implementation of absolute calibration. The implementation of the Bayesian probability theory for density error estimation and application of the code to fast measurement are further steps in the code development.

# Bibliography


[1] ANDA, G., PETRAVICH, G., ZOLETNIK, S. and BATÓ, S. *Li-beam developments for high-energy plasma diagnostics*. Fusion engineering and design, 2005, vol. 74, no. 1, p. 715–719.

[2] ANDA, G., BATÓ, S., ZOLETNIK, S. and PETRAVICH, G. *Li-beam ion source developments*. Annual Report 2004 EURATOM Association - Hungarian Academy of Sciences, 2004.

[3] BELL, K.L., GILBODY, H.B., HUGHES, J.G., KINGSTON, A.E. and SMITH, F.J. *Recommended data on the electron impact ionization of light atoms and ions*. Journal of physical and chemical reference data, 1983, vol. 12, p. 891.

[4] BERTA, M., BENCZE, A., ANDA, G., ARADI, M., DUNAI, D., VERES, G. and ZOLETNIK, S. *Concept of an Atomic Beam Probe diagnostic on COMPASS tokamak*. EPS Conference on Plasma Physics Sofia, 2009.

[5] BÍLKOVÁ, P., AFTANAS, M., BÖHM, P., WEINZETTL, V., ŠESTÁK, D., MELICH, R., STÖCKEL, J., SCANNELL, R., WALSH, M. *Design of new Thomson scattering diagnostic system on COMPASS tokamak*. Nuclear Instruments and Methods in Physics Research Section A: Accelerators, Spectrometers, Detectors and Associated Equipment, 2010, vol. 623, no. 2, p. 656–659.

[6] BRANDENBURG, R., SCHWEINZER, J., FIEDLER, S., AUMAYR, F. and WINTER, H.P. *Modelling of fast neutral Li beams for fusion edge plasma diagnostics*. Plasma physics and controlled fusion, 1999, vol. 41, p. 471.

[7] BRIX, M., KOROTKOV, A., LEHNEN, M., MORGAN, P., McCORMICK, K., SCHWEINZER, J., SUMMERS, D. and VINCE, J. *Determination of EDGE Density Profiles in JET using a 50kV Lithium Beam*. Proc. 28th EPS Conf. Controlled Fusion Plasma Physics, 2001, vol. 25, p. 389–392.

[8] COWAN, G. *Statistical data analysis*. Oxford University Press on Demand, 1998. p. 95–112.

[9] DERENIAK, E.L. and CROWE, D.G. *Optical radiation detectors*. New York: John Wiley and Sons, Inc., 1984.

[10] FIELDING, S.J., ASHALL, J.D., CAROLAN, P.G., COLTON, A., GATES, D., HUGILL, J., MORRIS, A.W., VALOVIC, M. and others. *The H-mode in COMPASS-D*. Plasma Physics and Controlled Fusion, 1996, vol. 38, no. 8, p. 1091.

[11] FISCHER, R., WOLFRUM, E., SCHWEINZER, J. and others. *Probabilistic lithium beam data analysis*. Plasma Physics and Controlled Fusion, 2008, vol. 50, no. 8, p. 085009.

[12] GRIEM, H.R. *Principles of plasma spectroscopy*. London: Cambridge University Press, 1998. p. 386.

[13] HACEK, P., WEINZETTL, V., STOCKEL, J., ANDA, G., VERES, G., ZOLETNIK, S. and BERTA, M. *Atomic Beam Probe Diagnostic for COMPASS Tokamak*. WDS 2010-Proceedings of Contributed Papers. Proceedings of the 19th Annual Conference of Doctoral Students, held 1-4 June 2010, in Prague, 2010, vol. 1, p. 7–11.

[14] HUTCHINSON, I.H. *Principles of plasma diagnostics*. Cambridge University Press, 2002. p. 322–367.

[15] KADO, S., OISHI, T., TANAKA, S. and others. *21st IAEA Fusion Energy Conference Proceedings*. 2006.

[16] JANEV, R.K., and International Nuclear Data Committee. *Atomic collision database for Li beam interaction with fusion plasmas*. IAEA Nuclear Data Section, 1993.

[17] KRAMIDA, A., RALCHENKO, Y., READER, J. and NIST ASD Team (2012). *NIST Atomic Spectra Database (ver. 5.0)* [Online]. National Institute of Standards and Technology, 2013. http://physics.nist.gov/asd

[18] KU, H.H. *Notes on the use of propagation of error formulas*. Precision Measurement and Calibration, 1969, vol. 1, p. 331–341.

[19] LAO, L.L., JOHN, H.S., STAMBAUGH, R.D., KELLMAN, A.G. and PFEIFFER, W. *Reconstruction of current profile parameters and plasma shapes in tokamaks*. Nuclear fusion, 1985, vol. 25, no. 11, p. 1611.

[20] MANDL, W., WOLF, R.C., VON HELLERMANN, M.G., and SUMMERS, H.P. *Beam emission spectroscopy as a comprehensive plasma diagnostic tool*. Plasma physics and controlled fusion, 1993, vol. 35, no. 10, p. 1373.

[21] MATHWORKS, INC. *Optimization Toolbox: User's Guide, Revised for Version 6.2.1* [Online]. Mathworks, Inc. 2012. http://www.mathworks.com/

[22] PÁNEK, R., BILYKOVÁ, O., FUCHS, V., HRON, M., CHRÁSKA, P., PAVLO, P., STÖCKEL, J., URBAN, J., WEINZETTL, V., ZAJAC, J. and others. *Reinstallation of the COMPASS-D tokamak in IPP ASCR*. Czechoslovak Journal of Physics, 2006, vol. 56, no. 2, p. B125–B137.

[23] PAPOULIS, A. *Probability, Random Variables and Stochastic Processes*, Mc Graw-Hill Kogakusha, 1965.

[24] PUSZTAI, I., POKOL, G., DUNAI, D., RÉFY, D., ANDA, G., ZOLETNIK, S., SCHWEINZER, J. and others. *Deconvolution-based correction of alkali beam emission spectroscopy density profile measurements*. Review of Scientific Instruments, 2009, vol. 80, no. 8, p. 083502–083502.

[25] PUSZTAI, I., DUNAI, D., POKOL, G., PÓR, G., SCHWEINZER, J. and ZOLETNIK, S. *Capabilities of alkali Beam Emission Spectroscopy for density profile and fluctuation measurements*. Proceedings of the 34th EPS Conference on Plasma Physics, Warszawa, 2007, vol. 31.

[26] ŠESTÁK, D., WEINZETTL, V., BILKOVA, P., BÖHM, P., AFTANAS, M., NAYDENKOVA, D., STÖCKEL, J., ĎURAN, I., and WALSH, M.J. *Design and engineering of optical diagnostics for COMPASS*. Fusion Engineering and Design, 2009, vol. 84, no. 7, p. 1755–1758.

[27] SCHWEER, B. *Application of atomic beams in combination with spectroscopic observation for plasma diagnostic*. Fusion Science and Technology, 2008, vol. 53, no. 2T, p. 425–432.

[28] SCHWEINZER, J. *Documentation on the Installation of a Code Package at NIFS for Reconstructing Density Profiles from Lithium Beam Emission Data*. Garching: MPI fur Plasmaphysik, 2005.

[29] SCHWEINZER, J., BRANDENBURG, R., BRAY, I., HOEKSTRA, R., AUMAYR, F., JANEV, R.K. and WINTER, H.P. *Database for inelastic collisions of lithium atoms with electrons, protons, and multiply charged ions*. Atomic Data and Nuclear Data Tables, 1999, vol. 72, no. 2, p. 239–273.

[30] SCHWEINZER, J., WOLFRUM, E., AUMAYR, F., POCKL, M., WINTER, H. SCHORN, R.P., HINTZ, E. and UNTERREITER, A. *Reconstruction of plasma edge density profiles from Li I (2s-2p) emission profiles*. Plasma physics and controlled fusion, 1992, vol. 34, p. 1173.

[31] SMIL, V. *Energy at the crossroads: global perspectives and uncertainties*. The MIT Press, 2005.

[32] SZAPPANOS, A., BERTA, M., HRON, M., PÁNEK, R., STÖCKEL, J., TULIPÁN, S., VERES, G., WEINZETTL, V., ZOLETNIK, S. *EDICAM fast video diagnostic installation on the COMPASS tokamak*. Fusion Engineering and Design, 2010, vol. 85, no. 3, p. 370–373.

[33] WAGNER, F., BECKER, G., BEHRINGER, K., CAMPBELL, D., EBERHAGEN, A., ENGELHARDT, W., FUSSMANN, G., GEHRE, O., GERNHARDT, J., GIERKE, G., and others. *Regime of improved confinement and high beta in neutral-beam-heated divertor discharges of the ASDEX Tokamak*. Physical Review Letters, 1982, vol. 49, no. 19, p. 1408–1412.

[34] WEINZETTL, V., PANEK, R., HRON, M., STÖCKEL, J., ŽÁČEK, F., HAVLÍČEK, J., BÍLKOVÁ, P., NAYDENKOVÁ, D., HÁČEK, P., ZAJAC, J. and others. *Overview of the COMPASS diagnostics*. Fusion Engineering and Design, 2011, vol. 86, no. 6, p. 1227–1231.

[35] WESSON, J. *Tokamaks*. New York: Oxford University Press, 1987. p. 237–290.

[36] WIESE, W.L. and FUHR, J.R.*Accurate atomic transition probabilities for hydrogen, helium, and lithium*. Journal of Physical and Chemical Reference Data, 2009, vol. 38, p. 565.

[37] WUTTE, D., JANEV, R.K., AUMAYR, F., SCHNEIDER, M., SCHWEINZER, J., SMITH, J.J. and WINTER, H.P. *Cross sections for collision processes of Li atoms interacting with electrons, protons, multiply charged ions, and hydrogen molecules*. Atomic Data and Nuclear Data Tables, 1997, vol. 65, no. 1, p 155–180.

[38] ZOHM, H. *Edge localized modes (ELMs)*. Plasma Physics and Controlled Fusion, 1996, vol. 38, no. 2, p. 105.

[39] ZOLETNIK, S., PETRAVICH, G., BENCZE, A., BERTA, M., FIEDLE, S., McCORMICK, K. and SCHWEINZER, J. *Two-dimensional density and density fluctuation diagnostic for the edge plasma in fusion devices*. Review of scientific instruments, 2005, vol. 76, no. 7, p. 073504–073504.